technologies

Review

Material Design for Enhancing Properties of 3D Printed Polymer Composites for Target Applications

Vinita V. Shinde [1,†], Yuyang Wang [1,2,†], Md Fahim Salek [3], Maria L. Auad [1,2], Lauren E. Beckingham [3] and Bryan S. Beckingham [1,*]

[1] Department of Chemical Engineering, Auburn University, Auburn, AL 36849, USA; vvs0004@auburn.edu (V.V.S.); yzw0104@auburn.edu (Y.W.); mla0001@auburn.edu (M.L.A.)
[2] Center for Polymers and Advanced Composites, Auburn University, Auburn, AL 36849, USA
[3] Department of Civil & Environmental Engineering, Auburn University, Auburn, AL 36849, USA; mzs0184@auburn.edu (M.F.S.); leb0071@auburn.edu (L.E.B.)
* Correspondence: bsb0025@auburn.edu
† These authors contributed equally to this work.

Abstract: Polymer composites are becoming an important class of materials for a diversified range of industrial applications due to their unique characteristics and natural and synthetic reinforcements. Traditional methods of polymer composite fabrication require machining, manual labor, and increased costs. Therefore, 3D printing technologies have come to the forefront of scientific, industrial, and public attention for customized manufacturing of composite parts having a high degree of control over design, processing parameters, and time. However, poor interfacial adhesion between 3D printed layers can lead to material failure, and therefore, researchers are trying to improve material functionality and extend material lifetime with the addition of reinforcements and self-healing capability. This review provides insights on different materials used for 3D printing of polymer composites to enhance mechanical properties and improve service life of polymer materials. Moreover, 3D printing of flexible energy-storage devices (FESD), including batteries, supercapacitors, and soft robotics using soft materials (polymers), is discussed as well as the application of 3D printing as a platform for bioengineering and earth science applications by using a variety of polymer materials, all of which have great potential for improving future conditions for humanity and planet Earth.

Keywords: additive manufacturing; polymer composites; self-healing polymers; energy-storage devices; bioengineering; porous media

Citation: Shinde, V.V.; Wang, Y.; Salek, M.F.; Auad, M.L.; Beckingham, L.E.; Beckingham, B.S. Material Design for Enhancing Properties of 3D Printed Polymer Composites for Target Applications. *Technologies* **2022**, *10*, 45. https://doi.org/10.3390/technologies10020045

Academic Editors: Jeng-Ywan Jeng and Ajeet Kumar

Received: 31 January 2022
Accepted: 7 March 2022
Published: 23 March 2022

1. Additive Manufacturing

Polymer and polymer composites can be fabricated using various manufacturing techniques. Conventional methods have limitations in polymer and composite manufacturing due to the need for precise molds for every single design and inability to manufacture complex and customized parts. Additive manufacturing (AM) has key advantages, as it allows for the production of customized and complex polymer composite parts in an economical way [1]. Additive manufacturing enables the production of complex part geometries generated by computer-aided 3D design with minimal material waste through the additive layer-by-layer fashion of manufacturing [1–3]. There are a variety of different additive manufacturing technologies, as shown in Figure 1, many of which have found use for rapid prototyping in different industrial applications [4,5].

Process	Acronyms	Feedstock	Material	Bonding and join
 Extrusion (or fused filament fabrication or fused deposition modeling)	FFF, FDM	Filament, rod, pellets	Polymer	Fused with heat
 Photopolymerization (or stereolithography)	SLA	Liquid	Photopolymer, metal, ceramics, composite	Cured with laser, projector, UV light
 Material Jetting (or Binder Jetting)	MJ (BJ)	Powder, liquid	Ceramic, wax, polymer, metal, sand	Cured with UV light, heat
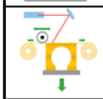 Laminated Object Manufacturing (or Sheet Lamination)	LOM	Sheet	Paper, metal, polymer	Joined with agent, heat and pressure
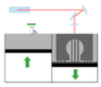 Selective Laser Melting	SLM	Powder	Metal	Fused with laser and electron beam
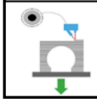 Directed Energy Deposition	DED, EBM	Wire, powder	Metal	Fused with laser and electron beam

Figure 1. Additive manufacturing processes. Reprinted (adapted) with permission from Ref. [5]. Copyright 2020. MDPI Materials.

1.1. Types of Additive Manufacturing

In this review, we aim to focus on unique applications of 3D printing technologies; thus, while the following is not focused on reviewing the various 3D printing technologies, the succeeding sections give a general overview of the primary technologies. For example, selective laser sintering utilizes thermal energy to fuse a material powder into a solid part on a printing bed in successive layers using high-temperature laser to construct the structure. This process is perhaps the least utilized for polymer materials; however, it has found use for polyamide polymer matrices with different types of fillers. For instance, Goodridge et al. have investigated the impact of carbon nanofiber (CNF) addition on the processing parameters and mechanical properties of laser-sintered parts [6]. The second type of additive manufacturing technique is vat polymerization. UV light is used to cure a photo-resin in a vat using either a laser (stereolithography) or 2D projector (digital light projection) to generate the structural pattern for each layer. These vat photopolymerization techniques are commonly used for printing polymer composites, where the polymer matrix materials are usually epoxy resin, polyester resin or acrylate resin [7–10]. Some advantages of this technology are the high resolution (25–100 µm) and smooth surface finish, which favor its application in constructing smaller and complex devices with high precision. However, drawbacks include the rather limited number and types of available resin materials as well as the high cost of high-performance resins.

The third type of process is through material extrusion. In material extrusion, filaments or material paste are extruded through a nozzle, and deposited on a build platform in the form of layers. The first category in the material extrusion process is liquid deposition modeling. In liquid deposition modeling, paste or liquid material is stored in a syringe and deposited selectively on a build platform based on the target design [1]. Shear thinning behavior is an important feature of material liquid deposition modeling, as the material must be extruded smoothly through the nozzle during the fabrication process but remain in place once deposited at the target locations [1]. While this technique is often cost-effective, it requires specific rheological and viscoelastic properties of the material, and agglomeration of the dispersed phase (in the case of composites) can lead to clogging of the nozzle [11]. Alternatively, inkjet printing is a similar process, in which an ink is released from a nozzle by piezoelectric action and the subsequent evaporation of solvent results in solidification of the material from the ink dispersion [12]. While both ceramic components and complex

polymer parts can be fabricated using inkjet printing [13,14], this process also requires tight control over the material dispersion and utilizes delicate extruder heads and expensive ink cartridges [12].

A second category of material extrusion is fused filament fabrication (FFF). Fused filament fabrication is a well-known technology for fabrication of prototypes and end-use parts of thermoplastic materials because of its simplicity, reliability, and affordability [15]. In FFF, thermoplastic materials are melted and extruded through a nozzle, subsequently cooling, and solidifying in place to form the targeted structure. The combination of the relatively broad variety of polymer materials and polymer composites compatible with FFF 3D printing and the fairly low cost of entry-level FFF printers has led to the popularity and comparably broader application of FFF 3D printing [16–19].

2. Materials Design for Inherent Properties

3D printing is a challenging process, as several factors are employed for achieving superior mechanical strength, including material design, printing parameters, and post processing. The following summarizes recent research on material design for 3D printing to improve mechanical performance of 3D-printed materials. Here, the literature on 3D printing of chopped and continuous carbon fiber-reinforced polymer composites is discussed as a primary route for improving mechanical strength/toughness. Additionally, recent research in 3D printing of self-healing polymer composites that allow materials to autonomously recover mechanical strength/toughness in response to a damage event is discussed, including different polymer systems and mechanisms used for fabricating self-healing polymer composites.

2.1. Carbon Fiber-Reinforced Polymer Composites (CFRP Composites)

Carbon fiber-reinforced composites consist of both matrix and reinforcement, where the matrix is a base material that supports the fibers and protects against external degradation and abrasion. Reinforcement in the polymer matrix synergistically improves material physical properties including elastic, flexure, tensile and load-bearing capacity. However, there are challenges to achieving the ultimate desired mechanical properties, such as the selection of polymer matrix and reinforcement material, as they must be compatible chemically (matrix and fiber should not react chemically), physically (good interfacial adhesion), and thermally (typically similar thermal behavior). Fused filament fabrication (FFF) is a very common technique to fabricate CFRP composites for applications ranging from prototyping to development of small to large functional parts that require high mechanical performance. The reason for its popularity is its ease of use and the low cost of the machines, process, and materials. As feedstock, FFF uses thermoplastic polymer materials that are of low toxicity and easy and safe to handle during processing. Thermoplastic polymer materials can be recycled after material failure, which makes them the common material of choice for 3D printing of polymer composites [20]. However, the main challenge of using FFF technology and thermoplastic materials is obtaining superior mechanical strength, as FFF uses the thermal fusion approach for 3D printing, which can lead to defects between printed layers and poor mechanical performance [21–23].

2.1.1. Carbon Fiber Filaments

Despite the availability of a variety of polymer materials for 3D printing, their mechanical properties such as stiffness and strength are typically lower than those of metal and fiber composites, limiting their use in high-performance applications. In addition, some of the 3D printing processes have inherent limitations in applicability and commonly result in voids within/between printed layers (an area of intense research and optimization), leading to comparably poor strength. Therefore, to widen the applicability of polymer materials for 3D printing, research on polymer fiber-reinforced and polymer matrix composites has recently grown. Carbon, glass, and Kevlar fibers are some of the most common reinforce-

ment materials used for polymer systems, where carbon fiber-reinforced composites in particular yield large improvements in mechanical performance.

One of the techniques used for addition of carbon fibers to a polymer system is laser sintering by using the polymer in powder form. For instance, Goodridge et al. demonstrated (stated in Section 1.1) the preparation of carbon nanofiber-polyamide 12 composite powder using the melt mixing and cryogenic milling technique, followed by laser sintering to fabricate polyamide composite structures, as shown in Figure 2A [6]. Addition of 3% carbon nanofibers resulted in an increase in the storage modulus value of polyamide composites by 22%. However, this technique is not commonly used commercially due to the lack of availability of polymer materials for 3D printing. Therefore, polymer filament preparation using short carbon fibers is a commonly adapted process to introduce reinforcement into polymer matrices due to their ease of fabrication, low cost, and superior mechanical strength as compared to polymer matrix itself. Generally, short-fiber compounded polymer filaments are made in two steps. Polymer pellets are first mixed in a mechanical blending process with short carbon fibers, and then this compounded material blend is melt-extruded to form filaments.

Several researchers have utilized this type of process to produce composite filaments and investigated the addition of short fibers into thermoplastic polymers as polylactic acid (PLA), acrylonitrile butadiene styrene (ABS), polyether ether ketone (PEEK), polypropylene (PP), and nylon (polyamide) to fabricate composite filaments [22]. The reported investigations included the impact of fiber length and orientation on physical characteristics of 3D-printed fiber-reinforced polymer composites. Ning et al. investigated effects of carbon fiber content and length on the mechanical properties and porosity of 3D-printed CFRP composites [24]. As shown in Figure 2B, ABS polymer pellets were used along with carbon fibers to extrude carbon fiber-reinforced filaments, followed by 3D printing of CFRP ABS matrix composites. The addition of carbon fibers in the ABS polymer system increased tensile and flexure strength but decreased toughness. Moreover, with an increase in the content of carbon fiber up to 10 wt.%, porosity increased due to the increasing physical gap between 3D-printed layers resulting from the variance in carbon fiber distribution and inconsistent thermal fusion of layers at the interface [24]. Ferreira et al. studied reinforcement of short-length carbon fibers with PLA to investigate the mechanical characterization of 3D-printed composites produced by FFF [25]. It was concluded that the incorporation of short carbon fibers in PLA increased tensile modulus by two times, and carbon fibers remained aligned with the length of the 3D printing filament and also in the direction of 3D printing, which helped in improving the stiffness of the composite structure [25].

Another strategy to improve the strength of the thermoplastic material using FFF is the development of new printing methods such as 3D printing of continuous carbon fiber-reinforced polymer composites. Yao et al. made great efforts in 3D printing continuous carbon fiber-reinforced PLA composites using FFF, where carbon fibers are separately impregnated with epoxy resin to place them on the first few 3D-printed layers, and then composite structures are produced on laid carbon fibers with the extruded PLA (shown in Figure 2C; process demonstrated as (a–h)) [26]. This method not only improved tensile strength of PLA composites by 70% but also reduced the weight of materials used for 3D printing by approximately 11%. Moreover, carbon fibers in the composite microstructures also served as sensory agents by monitoring changes in the electrical resistance of the fiber due to deformation (more information about self-monitoring devices is in Section 3) [26]. However, challenges remain for the use of continuous carbon fibers, such as enhancing adhesion between the carbon fibers and thermoplastic polymer to obtain better reinforcement. Moreover, advances in functional nanomaterials, which can be included in the ink, have led to the rapid development of printed electronics and prototypes (more information in Section 3.2.1). Kim et al. studied 3D printing of microstructures containing approximately 75 wt.% of carbon nanotubes and 25% polyvinylpyrrolidone (PVP) as a stabilizer and rheology modifier, as shown in Figure 2D [11]. A high concentration of multiwalled carbon nanotubes (MWNT) was added to achieve excellent thermal and electrical properties in

meniscus-guided 3D-printed microstructures along with superior mechanical strength [11]. They showed that fabrication of highly conductive microstructures is possible with the utilization of only MWNT ink and evaporation of PVP by thermal treatment during 3D printing.

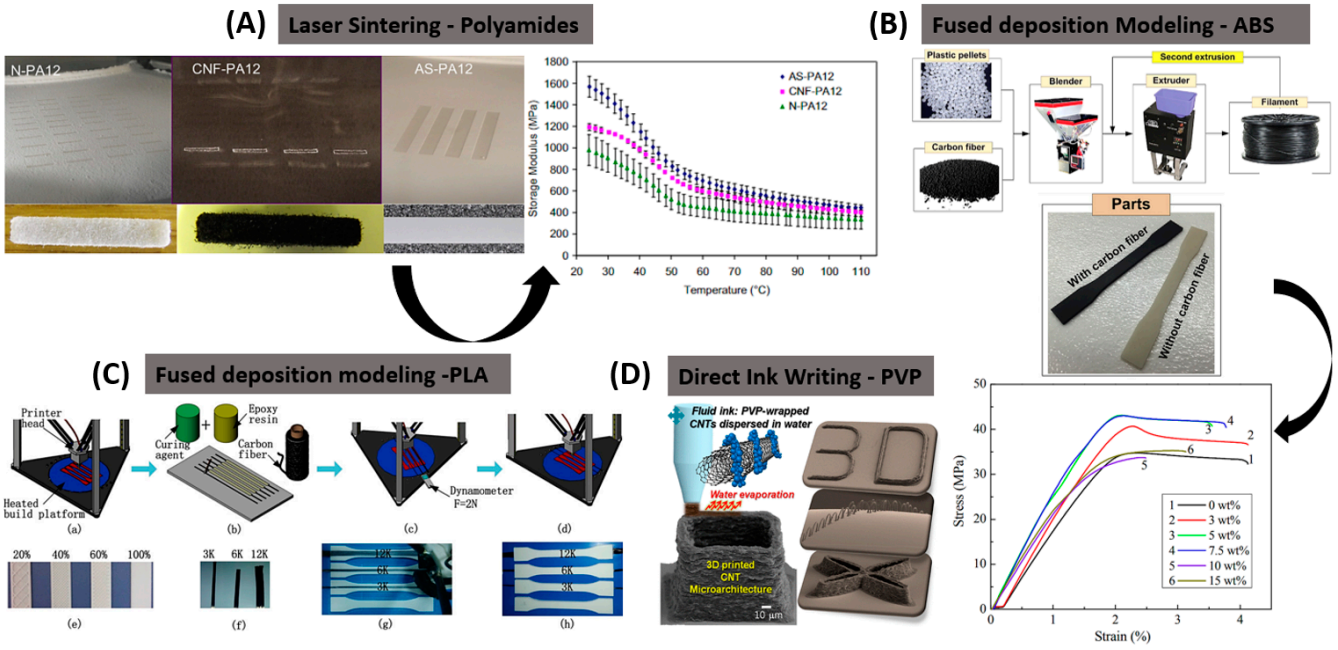

Figure 2. (**A**) Laser sintering of carbon-fiber-reinforced polyamide material and its mechanical characterization. Reprinted (adapted) with permission from Ref. [6]. Copyright 2010 Elsevier. (**B**) Fabrication of carbon-fiber-reinforced ABS filaments using melt extrusion and FFF 3D printing of ABS composites. Reprinted (adapted) with permission from Ref. [24]. Copyright 2015 Elsevier. (**C**) FFF 3D printing of carbon-fiber-reinforced PLA composites using continuous carbon fibers impregnated using epoxy resin and embedding pre-peg carbon fibers on 3D printed PLA layers with process demonstrated as (a–h). Reprinted (adapted) with permission from Ref. [26]. Copyright 2017 Elsevier. (**D**) 3D-printed MWNT microarchitecture is printed by horizontally pulling a micronozzle filled with CNT ink (PVP-wrapped A-MWNT suspended in water). Reprinted (adapted) with permission from Ref. [11]. Copyright 2016 American Chemical Society.

Besides improving technology and materials, researchers are also trying to fabricate carbon fiber-infused polymer filaments prior to 3D printing. Recently, a new class of polymer materials was introduced, namely Onyx and ABSPlus [27,28]. Onyx is a carbon fiber-reinforced tough nylon filament, combining the tensile strength and thermal properties of carbon fibers with the toughness of nylon. Yasa et al. evaluated the mechanical properties and dimensional accuracy of carbon fiber-reinforced nylon composites produced with the fused filament fabrication technology [29]. The study showed that adding carbon fibers into the nylon matrix improved yield strength and modulus compared to nylon without any reinforcement. These materials are considered for specific industrial applications where both toughness and strength are required. Another new 3D printing polymer material class is ABSPlus, which minimizes the sensitivity of acrylonitrile-butadiene-styrene (ABS) polymer to shrinkage and warping while preserving most of its mechanical properties. Rybachuk et al. investigated the anisotropic mechanical properties of fused filament fabricated parts produced using ABSPlus polymer [30]. The study showed improvement in the mechanical properties of the ABSPlus parts with the orientation aligned to the vertical axis (z-axis) while 3D printing [30].

2.1.2. Carbon Fiber Resins

Another approach is using carbon fiber within polymer resins employing 3D printing to fabricate thermosetting composites. Continuous carbon-fiber-reinforced thermoset polymer composites show better mechanical performance than thermoplastic polymer composites because of the chemical reaction occurring at the fiber and polymer matrices' interface [26]. Materials used for thermosetting composites are epoxy resins and carbon fiber bundles where carbon fibers are passed through an epoxy resin pool that directs towards the printing head for extrusion during printing. Once the sample is printed on a building platform, it is subjected to high temperatures for thermal curing [27]. For example, Hao et al. studied 3D printing of continuous carbon fiber-reinforced thermosetting epoxy-based composites using FFF and observed superior mechanical strength of the composite structures as compared to carbon fiber-reinforced thermoplastic composites [27]. Rahman et al. also studied 3D printing a UV-curable resin reinforced with continuous carbon fibers and observed that the composite structures had superior mechanical performance and excellent thermal stability due to the crosslinked nature of the material with higher load-bearing capacity due to dispersion of continuous carbon fibers in the polymer matrix [28]. However, due to the fundamental mechanisms of stereolithography 3D printing, reinforcing polymer material with continuous fiber is still a challenge. Therefore, a more common way to 3D print thermoset composites using photopolymerization is to use short carbon fibers, as using continuous fibers for thermoset resin 3D printing is still relatively new. The mechanical properties of short fiber-reinforced SL printed parts largely depend on the alignment of the short fibers. Shear aligning of the short fiber has also been investigated. Yunus et al. [31] induced shear aligning by the movement of the vat relative to the build plate. Improved fiber alignment in 3D printing matrix material can result in excellent mechanical performance; in this case flexural properties of SLA-printed composites improved by 90% compared to randomly distributed samples [31].

2.2. Self-Healing

All engineered materials are susceptible to deterioration, damage, and failure [32]. Damage in a material can occur during its processing, due to accidental external events or by wear and tear during use [33]. Additionally, the combined impacts of heat, light, chemical medium, and environmental factors can lead to the degradation of materials [34]. In nature, biological systems address this issue by self-healing, where the overall goal of living systems is to survive, and healing is the primary option used by animals and plants [27,29]. This influential biological self-healing concept has inspired scientists to incorporate similar functionality within synthetic materials to build "self-healing materials" [35,36]. Self-healing is an intrinsic ability of a material to repair damage (partially or completely) and recover its lost or degraded physical properties and functional performance using the resources inherently available to the material systems [27,31,32]. Self-healing thereby aims to increase the robustness and prolong the service life span of a material when repair or replacement of the material is economically not affordable, not possible, or unsafe [33,37–39]. The following sections describe self-healing polymer systems that repair injuries without human intervention, as inspired by living materials, and their application to 3D printing of polymer composites [33].

2.2.1. Types of Self-Healing

Self-healing can either be an autonomous process where external intervention is not required, or it can be non-autonomous, where external force, heat [39,40], organic solvents [41–43], or UV-light [41,42] is necessary to initiate the process. Autonomous self-healing does not require external stimulus to initiate the healing because the material damage itself is enough to trigger the process [44–51]. Autonomous self-healing is valuable in difficult-to-access environmental conditions, e.g., inside devices such as implants, deep sea pipelines, and aerospace applications [35]. Self-healing systems can be further categorized into two primary conceptual approaches: intrinsic and extrinsic. In intrin-

sic self-healing, the material itself incorporates the ability to heal via reversible bonding, typically in presence of heat or UV-light, whereas in extrinsic self-healing, this ability is incorporated through the addition of a second material such as a microcapsule or microvascular network with autonomic self-healing ability [33]. The type of self-healing approach and its implementation impact the damaged volume that can be repaired, the repeatability of healing at the same location, and the speed at which the healing occurs [33].

Intrinsic Self-Healing

Intrinsic self-healing materials recover from a damage event through inherent reversible bonding or reversible reactions in the polymer matrix [33,51]. Intrinsic self-healing does not require the addition of an external healing agent, avoiding many issues with incorporation of healing systems in the material and their compatibility with the material [33]. One common route to intrinsic self-healing materials is through reversible reactions, such as reversible polymerization of crosslinking where the polymer itself can be reversed to its monomeric or un-crosslinked state during the damage event and subsequently repairs itself autonomously or by utilizing external stimuli such as heat or light [52]. Intrinsic self-healing systems are capable of multiple healing events due to the repeatability of the utilized reversible reactions. However, as intrinsic self-healing systems mostly rely on external stimulus (heat or light), their application space is limited somewhat to material-specific temperature windows or application-specific accessibility to light [53].

One example of reversible reaction-based intrinsic self-healing is through Diels–Alder cycloaddition [40,41,54–60]. Intrinsic self-healing has also been demonstrated utilizing ionomer chemistries such as poly(ethylene-co-methacrylic acid) [51,53], where thermally assisted ionic interactions near the crack area lead to formation of clusters of ionic segments, resulting in self-healing [60]. Additional routes to intrinsic self-healing include incorporation of reversible hydrogen bonds [61,62] and molecular diffusion [63]. Intrinsic self-healing systems are capable of multiple healing events due to reversible reactions. However, a majority of the studies in intrinsic self-healing systems are limited to thermoplastic polymers, which restricts their application for heavy-duty systems due to their low strength, stiffness and low T_g [53]. Intrinsic self-healing systems mostly rely on external stimulus, limiting their application in difficult-to-access conditions [53], thus motivating further studies on the development of intrinsic self-healing systems without external stimulus requirements or easily available external stimulus [53].

Extrinsic Self-Healing

Extrinsic self-healing is a type of autonomous healing, where healing fluids are incorporated in the form of capsules or vascular networks that are isolated in a separate phase from the host material. Extrinsic self-healing systems contain encapsulated containers in the form of capsules or vascular networks that release a healing fluid during the crack event and initiate the self-healing process [64].

Capsule-based self-healing materials are one category of extrinsic self-healing, where a healing fluid is stored inside discrete microcapsules [37]. Microcapsules are micron-sized particles consisting of one or more core reactive materials surrounded by single or multiple shell walls [65]. When these capsules are ruptured by a propagating crack, the self-healing process initiates due to the release of healing fluid and subsequent reaction near the crack plane. Microcapsule-based self-healing systems are highly localized systems and can heal the crack right where it is initiated, but their main drawback is that they are restricted to single damage events at a given site [66]. Additionally, the healing fluid is depleted after this one release, leading to a singular local healing event [67]. Reactive materials are encapsulated using various techniques including in situ interfacial polymerization, melt dispersion, or coacervation. In-situ and interfacial emulsion polymerization are common encapsulation techniques due to their simplified process, as described below [49,50,64].

Microcapsule-based self-healing systems can be implemented using different methods of sequestering the healing agent(s). The first is a capsule-catalyst healing system,

where the healing fluid is an encapsulated monomer, and a corresponding catalyst is dispersed in the polymer matrix. White et al. [37] demonstrated for the first time dicyclopentadiene (DCPD)-Grubbs' first-generation catalyst-based self-healing system based on ring-opening metathesis polymerization. These capsule-catalyst-based systems have been incorporated into epoxy matrices [67,68] and epoxy composites [69] due to the ability of poly(dicyclopentadiene) to form cross-linked networks across the damage front, leading to high healing efficiency [68]. Another related approach is a multi-capsule system in which both core fluid and catalyst are encapsulated separately and both microcapsules are incorporated into the composite. Multi-capsule self-healing of elastomers has been reported by Keller et al., where platinum catalyst and poly(dimethylsiloxane) (PDMS) monomer were encapsulated separately in different microcapsules and dispersed in a PDMS resin matrix to produce a self-healing composite material [70]. Another capsule-based system utilizes a latent functionality of the polymer matrix itself, where microcapsules containing healing fluid are dispersed in the polymer matrix, and during the crack event, this incorporated functionality initiates the polymerization upon release of the healing fluid. Self-healing coatings are a great example of capsule-based systems utilizing latent functionality [71]. A different approach utilizing a latent system characteristic is solvent-based self-healing [72]. In solvent based self-healing systems, the healing fluid is a solvent that utilizes solvation of the bulk polymer to initiate the self-healing. In a solvent-based system, a crack in the polymer matrix releases the solvent to the crack site, locally dissolving the polymer and leading to re-bonding of the crack surfaces of the polymer matrix on evaporation of the solvent [73].

Vascular self-healing materials comprise a second category of extrinsic self-healing. Vascular self-healing materials operate analogously to the above-described capsule-based systems; however, they store and distribute the healing fluid through capillary-sized hollow tubes in the form of an interconnected network within the material [74]. For instance, vascular channels can be incorporated using hollow glass fibers [75]. Vascular networks with multiple connectivity have been prepared to have a larger accessible reservoir of healing fluid and to attain easier refilling of the fluid after depletion [66]. A key advantage of vascular self-healing system is their ability to achieve repetitive healing of damage events due to the high volume fraction of healing fluid and interconnected delivery through the network [76]. However, these systems can also suffer channel blockages that can restrict healing fluid access to new crack sites; fractured channels can lead to large-scale leakage that can soften the polymer matrix (plasticization); and the incorporation of interconnected vascular networks can be a complex endeavor [76].

2.2.2. Additive Manufacturing of Self-Healing Polymer Composites

As discussed above, thermoplastics and thermoset materials have been used to fabricate polymer parts or composite parts using different additive manufacturing technologies due to the easy accessibility of 3D printers and the ability to create complex and customized part in an economical way. Thermoplastics are a popular choice for additive manufacturing due to their flexibility, manageable melting temperature, fast cooling rates and user-friendly safe processing [77]. Poly(lactic acid) (PLA) is a common polymer used for 3D printing due to its biocompatibility, renewability and low extrusion temperature, which favor its application in biomedical industries [78]. Fabrication of PLA and PLA composites using FFF has been reported [79]. High-impact polystyrene (HIPS) is another polymer commonly used for 3D printing applications due to its easy fabrication and machinability [79]. HIPS has various benefits as a 3D printing material due to its high impact strength, high dimensional stability, and low cost. It is used on a large scale to fabricate prototypes for design validation. It is also used as a support material during 3D printing of complex parts containing overhangs and bridging. Compared to traditionally constructed parts, the main challenges faced by 3D-printed thermoplastic materials are poor mechanical properties, poor interlayer adhesion and delamination, which in the long term can lead to material failure. For these reasons, thermoplastics are genuine contenders for self-healing applica-

tions using additive manufacturing technologies. The concept of additive manufacturing of self-healing composites is still new. For self-healing of thermoplastic materials, Villajos et al. reported on poly(ethylene-co-methacrylic acid) (EMAA) copolymers reinforced with carbon nanotubes for 3D printing of self-healing composites [77].

Thermoset polymers are a second category of polymer composite. Thermoset polymers in the form of epoxy and acrylate resins are popularly used for fabricating composite materials due to their excellent mechanical stability at elevated temperature, good chemical resistance, and compatibility with commercial 3D printers [80]. However, in the case of thermoset materials, it is not generally possible to recycle or reshape thermosets if they develop damage. Moreover, in the case of a thermoset polymer material, the brittle nature and high crosslinking density of materials can result in catastrophic failure upon damage. Therefore, researchers are trying to find ways to combine self-healing and 3D printing technologies for repairing damage in thermoset polymer materials. Yu et al. studied self-healing properties in elastomers by incorporating thiol and disulfide groups within the structure, which undergo reversible reactions enabling healing upon the addition of force (0.5 N), as shown in Figure 3A, [81]. Liu et al. studied self-healing in a 3D-printed double-network of polyacrylamide (PAAm) in the presence of k-carrageenan (Figure 3B), and demonstrated repair of fractures upon heating the samples at high temperature [82].

There are some limitations with the 3D printing of hydrogel-based intrinsic self-healing systems, as they depend on external stimulus. Therefore, research on 3D printing of autonomous self-healing polymer systems has been conducted, and several studies have been reported. In 2019, Sanders et al. reported on the self-healing of stereolithographic 3D printing of thermoset composites using the solvent welding mechanism, where self-healing of photocured commercial resin was shown using anisole (solvent) filled microcapsules with 87% fracture recovery, as shown Figure 3A [83]. However, this route is dependent on the solubility of the polymer matrix in the solvent, and therefore, a more approachable and viable route was investigated by Shinde et al. [50]. In their study, Shinde et al. investigated stereolithographic (SLA) 3D printing of a self-healing composite system consisting of a commercial photocurable resin with embedded catalyst (Grubbs') and microcapsules containing dicyclopentadiene (DCPD) monomer. The study also provided a versatile platform for SLA 3D printing of self-healing thermoset polymer materials, as it does not require manipulation of the resin chemistry and has less reliance on solvent for fracture recovery, as shown in Figure 3C [50]. Another route is designing vascular self-healing networks as explained by Postiglione et al., where self-healing polymers based on embedded microvascular networks are 3D-printed, and resin material is stored in individual microchannels, which upon damage release the material, which then diffuses through and heals the cracks at microscopic and macroscopic levels, as shown in Figure 3D; where (a–h) represent images of vascular microchannels and its self-healing after crack event [84].

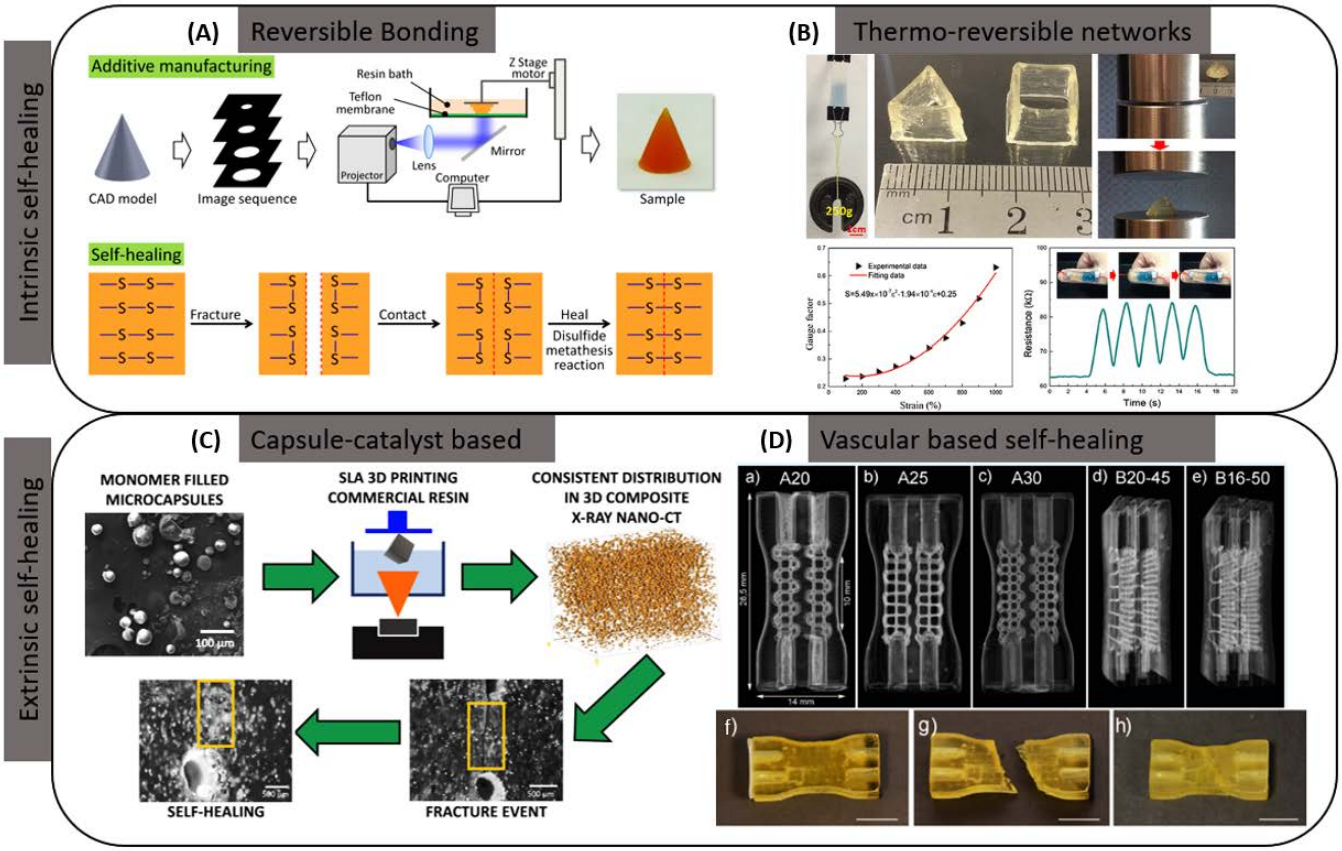

Figure 3. (**A**) Stereolithography 3D printing of self-healing thiol-based elastomer system, showing disulfide bond-assisted self-healing process. Reprinted (adapted) with permission from [81]. Copyright 2019. (**B**) Direct ink writing of polyacrylamide (PAAm) based hydrogel-based self-healing system in presence of k-carrageenan. Reprinted (adapted) with permission from [82]. Copyright 2017 American Chemical Society. (**C**) Stereolithography 3D printing of autonomous self-healing microcapsule-based polymer composite system. Reprinted (adapted) with permission from [50]. Copyright 2020 American Chemical Society. (**D**) Dual extrusion 3D printing of micro-vascular networks using PVA polymers to design self-healing vascular based system where (a–h) represent images of vascular microchannels and its self-healing after crack event. Reprinted (adapted) with permission from [84]. Copyright 2017 American Chemical Society.

3. Soft Robotics

Soft robotics is a specific branch of robotics that utilizes soft materials (polymers) and is inspired by natural living animals, including the octopus, elephant, spider, snake, and many others. Flexible and soft robotics are generally very adaptive to the working environment, assisting humans or replacing humans in many complex and dangerous situations, such as moving forward inside an irregular tunnel, performing surgeries, and grasping fragile objects. Compared to robotics with rigid constituents, soft robotics does not require wire control or motor actuation in response to various stimuli. The structure of soft robotics generally includes three components: soft actuators, sensors, and a control system. Here, we focus on leveraging 3D printing techniques for soft actuators that can deform under different types of environmental stimulation, including fluidic (hydraulic and pneumatic) and field-driven (chemical, electric, and magnetic) methods (Figure 4). More examples are also presented in Table 1.

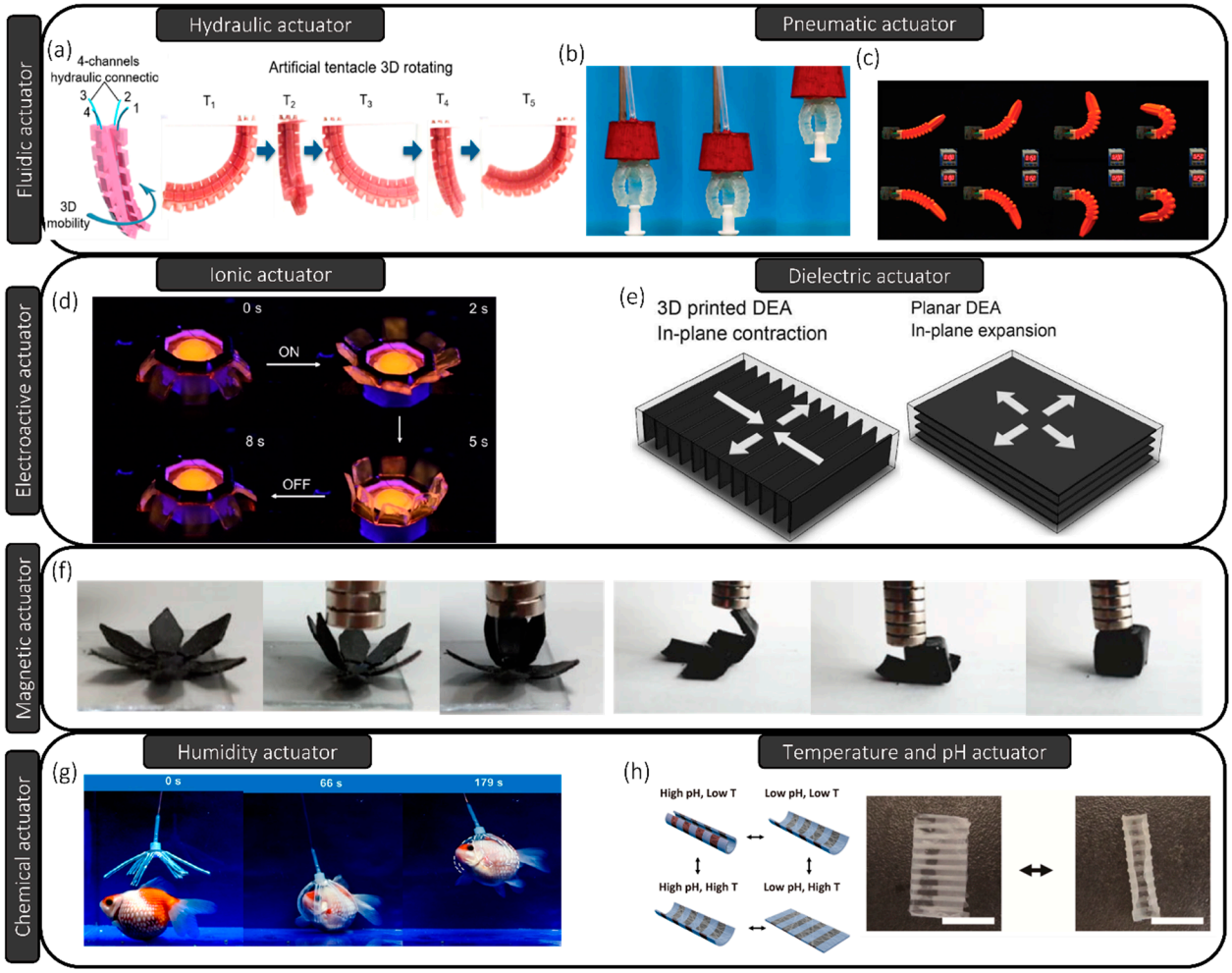

Figure 4. (**a**) DIW printed hydraulic actuator with time-dependent water injection. Adapted with permission from Ref. [85]. Copyright 2019 American Chemical Society. (**b**) DLP printed pneumatic gripper. Adapted with permission from Ref. [85].Copyright 2015 John Wiley and Sons. (**c**) FFF printed dual-channel pneumatic actuator. Adapted with permission from Ref. [86]. Copyright 2016 Mary Ann Liebert, Inc. (**d**) DIW printed jellyfish ionic actuator. Adapted with permission from Ref. [87]. Copyright 2021, American Chemical Society. (**e**) In-plane contraction and expansion of 3D printed DEA. Adapted with permission from Ref. [88]. Copyright 2019 John Wiley and Sons. (**f**) 3D printed flower with magnetite fillers enclosed under magnetic field. Adapted with permission from Ref. [89]. Copyright 2019 John Wiley and Sons. (**g**) A DIW printed humidity-responsive hydrogel actuator is grabbing a goldfish. Adapted with permission from Ref. [90]. Copyright 2020 American Chemical Society. (**h**) SLA printed gradient structure responsive to pH and temperature. Adapted with permission from Ref. [91]. Copyright 2022 Chemical Engineering Journal.

Table 1. Summary of literature reporting 3D-printed soft robotic structures.

Paper	Materials	Process	Structure	Parameters	Mechanical Properties	Application	Comments
Patel et al., 2017 [85]	Photocurable elastomer resin	DLP	3-legs gripper	70 °C bath, 385 nm; 10 s/ layer	E = 4.21 MPa ε = 1100%	Pneumatic actuator	DLP-printed elastomer has good potential in sealed hollow structures
Cheng et al., 2019 [84]	Low-viscosity hydrogel	DIW	4-channel tentacle	η = 50 Pa·S at 0.01 s^{-1}	E = 59.6 KPa Toughness = 424.6 KJ·m^{-3}	Hydraulic actuator	Hydrogels with abundant functionalities facilitate the free design of soft robotics
Wang et al., 2021 [87]	Dielectric elastomer	DIW	Jellyfish	216 Pa·S at 0.01 s^{-1}	E = 26.4 KPa Strength = 235.8 KPa	Electrically responsive gel actuator	3D-printed dielectric elastomer can actuate rapidly but requires high voltage
Kokkinis et al., 2015 [92]	Polymer-alumina composites	MM-3D [a]	Cuboids	1.15 Pa·S	E = 7 MPa ε = 150%	Magnetic actuator	MM-3D allows designing composites
Odent et al., 2019 [93]	Photocurable hydrogel resin	SLA	Gradient-like structures	3 s/layer (100 µm); 405 nm	-	Temperature-responsive actuator	3D-printed gradient structures have various volume expansion properties
Zhou et al., 2019 [94]	Dielectric elastomer	FFF	4-leg soft gripper	230° nozzle temperature, 100% filling density	Toughness = 440 J/m^2	Dielectric elastomer soft actuator	FFF aids the combination of multi-layer structures without using adhesives
Wang et al., 2018 [95]	Graphene/PDMS [b] composites	DIW	Grid/triangular porous/hexagonal porous structures	η = 10,000 Pa·S at 0.01 s^{-1}	-	Strain/temperature sensor	3D printing facilitates the design of complex structures of composites
Kalsoom et al., 2020 [96]	Polymer–particles–salt composites	FFF	Filaments	245 °C extrusion temperature; 0.8 mm nozzle	-	Humidity sensor	FFF facilitates composite sensors without additional electrode layers
Mu et al., 2017 [97]	Photocurable resin–carbon source composites	DLP	Hollow structure truss	η = 11.5 Pa·S at 1 s^{-1}; 40 s/layer (19.05 µm)	E = 10 MPa ε = 10%	Strain sensor	DLP optimized electrical performance by printing complex structures
Shen et al., 2018 [98]	Metal oxide and quantum dots	DIW	Symmetric arrays	>10^4 Pa·S at 10 s^{-1}	-	Micro-supercapacitors	Low-cost and efficient 3D printing optimized the process of building multilayer supercapacitors

Table 1. *Cont.*

Paper	Materials	Process	Structure	Parameters	Mechanical Properties	Application	Comments
Park et al., 2018 [99]	Photocurable resin and nanowires	DLP	Porous symmetric arrays	405 nm; 30 μm per layer; η = 1.3 Pa·S	-	Micro-supercapacitors	DLP helps achieve low electrical resistance by designing structural octet effect
McOwen et al., 2018 [100]	Ink (ceramic powder and polymer binder)	DIW	Symmetric arrays	η = 1500 cP	-	Solid-state lithium-ion batteries	Modification of ink formulations optimizes the solid-state electrolyte structure, enhancing electrochemical properties
He et al., 2020 [101]	Photocurable resins with ionic liquid	SLA	Growth rings	355 nm UV (10 W cm^{-2})	-	Solid-state lithium-metal batteries	3D-printed growth rings increase the specific area, loading more active materials.
Ayan et al., 2020 [102]	Electrocytes with mouse fibroblast cell line	Hybrid bioprinting	Heterogeneous pyramid with spheroids	250 μm nozzles	-	Precise positioning of biologics	Bioprinting aids study of tissue–tissue, tissue–material interactions and realize bottom-up assembly

[a] Multimaterial magnetically assisted 3D printing system. [b] Polydimethylsiloxane.

3.1. Fluidic Actuation

Fluidic actuation-based soft actuators (FSAs) contain built-in channels that can inflate with an applied purging pressure, including hydraulic or pneumatic pressure, resulting in a designed manipulation based on the structure. FSAs require materials with high elastic modulus, good toughness, and moderate stiffness, such that room-temperature vulcanized elastomers are widely used due to their flexibility and durability. However, unreinforced elastomers generally finalize with poor tear resistance. Research on materials for FSAs has accordingly focused on finding suitable elastomeric candidates, including silicone-based polydimethylsiloxane (PDMS), polyurethane (PU), and various hydrogels. Two-dimensional (2D) fabrication methods, such as casting liquid monomers into a model, followed by polymerization to form the desired solid shape, can limit the design of soft actuators. Three-D printing techniques, including DIW, DLP, and SLA, can fabricate FSAs using 3D printable materials to achieve complex geometries. For instance, Patel et al. 3D-printed a 3-arm gripper with hollow-ladder structures by photocuring UV-curable elastomers using DLP. The epoxy aliphatic acrylate-based elastomer actuator showed large elongation (1100% strain), allowing significant inflation with water and gas [85].

3.1.1. Hydraulic Soft Actuators

Hydraulic power is a type of closed-circuit drive system that applies liquid as a medium. Various deformations can take place by pulsing the hollow fluidic channels. The hydraulic pressure can generate considerable power and force, which can be applied in medical and bionic applications. For instance, Katzschmann et al. designed and simulated a fish-like robot that utilized hydraulic power for propulsion [103]. Hydraulic transmission tubes have also been embedded within composite fibers to fabricate artificial muscle systems. Zhu et al. have demonstrated wearable soft robotics based on sheets containing such fluidic fabric muscles, which utilized composite fabrics with elastic channels [104]. However, complexity in modeling, controlling, and planning for safe human–robot interactions remain formidable challenges. To eliminate the complicated assembly of soft actuators' discrete counterparts, Robert et al. designed and precisely controlled hydraulic actuators with hexapod, bellows, gripper, and gear pump structures based on the Inkjet printing technique. These hydraulic actuators have shown good mechanical strength, fatigue resistance, and high printing resolution [105]. To achieve safer and biocompatible interactions with human bodies, 3D-printed biocompatible hydrogels have been developed. The DIW technique has printed a biocompatible hydrogel actuator based on acrylamide (AAm) and alginate. The hydrogel network's ionic crosslinking and covalent crosslinking have functionalized the hydraulic hydrogel actuator with high toughness and good flexibility [85]. To realize precise controllability of soft hydraulic actuators, soft valves should be manufactured. Soft valves are attached to the soft actuators as a power source, driving or controlling the fluidic flow into the hollow tunnels of actuators. In other words, soft valves can act as a control system that regulates the flow rate, pressure, and mass, customizing the desired locomotion and output force of soft actuators. However, traditional hydraulic valves are fabricated from rigid materials, which present a major challenge in producing soft valves. Alex et al. designed an entirely soft hydraulic valve to replace the rigid valves in robotic systems based on the polyjet printing technique [106]. A printed octopus structure was composed of a valve, bellow-like legs, and an electrorheological fluid that facilitated controlled manipulation under the activation voltage.

Further investigations have focused on hydraulically amplified electrostatic actuators with self-healing properties because they have a high degree of freedom (DOF), including changing shape, modifying output power, and achieving desired stiffness under a controlled electric field. To develop a complex architecture of muscular hydrostats that shows various flow directions in the actuator, Maura et al. demonstrated an electrohydraulic tentacle actuator based on the CLIP method by photocuring silicone-urethane elastomers. The printed actuator showed a maximum of 460 mN with LiCl salt as conductive medium [107].

3.1.2. Pneumatic Soft Actuators

Pneumatic soft actuators (PSAs) are one of the essential fluidic actuators that can convert the pressure of compressed gas into the mechanical propulsion of controlled parts. The advantages, including ease of control, fast response, enormous output power, and safe interaction between humans and robotics, have generated numerous applications for PSAs in soft robotics, medication, and bioengineering. Pneumatic artificial muscle (PAM), also named McKibben actuator, has been one of the most popular applications of PSAs [108]. The composition of PAMs includes flexible elastomer tunnels and fiber sleeves, called Pneu-Nets (PN), which can achieve deformation with a high degree of freedom (DOF). However, one of the challenges of PNs is that they require complex fabrication and assembly procedures to realize high DOF. To solve the challenges and develop PSAs with high DOF that can realistically mimic the movement of biological creatures, such as octopuses, Bryan et al. designed a pneumatic octopus tentacle with great diversity in 3-dimensional (helical, longitudinal, and transverse) deformation based on the SLA technique [109]. The typical configuration of a PSA is of a balloon type that is easily formed by two elastomer layers and a cantilever to create a chamber inside. The challenge is that the bellow-type actuators have inefficient bending and low DOF. To solve this challenge, Benjamin et al. designed a novel fold-based structure for a PSA based on the DIW technique, showing a high force output at a safe pressure (<200 kPa) [110]. Hong et al. designed a dual-channel bellow-type actuator based on the FFF technique to achieve high DOF of the bending deformation [86].

The challenge of working with DIW and FFF utilizing thermoplastic materials is the limited selection of flexible filaments. The stiffness of thermoplastics can significantly reduce the gas pressure, impacting the output power. Moreover, the defects, including failures and holes in printed structures, can deflate the pneumatic chambers. Thus, high-resolution products were desperately needed to solve the voids and defects of pneumatic actuators. The DLP technique that utilizes the free radical polymerization method is an ideal method to print PSAs with closed systems and valves or channels with precisely controlled dimensions, because the unreacted monomers in each layer can also polymerize to eliminate the defects. DLP can even print PSAs on a microscale with high resolution and good mechanical properties. Zhang et al. 3D-printed a miniature PSA, such as a one-channel bellow-type, miniature 3-arm gripper, and bars with built-in chambers at millimeter-scale by introducing and adjusting the concentration of photo absorber in precursor inks using epoxy aliphatic acrylate (EAA) photocurable elastomer based on DLP [111]. Another way to solve the defects in DIW-printed samples is to introduce multi-material systems incorporating nanoparticles in the printable ink to functionalize the PSA, enhance the mechanical properties, and conduct heat more efficiently to improve the printing quality. A good demonstration is that of Zhang et al., who printed a flexible conductive circuit by utilizing an ink with silver nanoparticles that locally achieves fast heating. The printed PSA showed increased high load capacity, shape adaptivity, and fast heating–cooling [112].

One of the most critical advantages of vat polymerization printing techniques, including DLP, SLA, and CLIP, is the wide selection of materials available for synthesizing elastomers based on free radical polymerization. Apart from typical PU-based [85] and PDMS-based elastomers [113], hydrogel elastomers can also provide opportunities to print PSAs [114].

3.2. Field-Driven Soft Actuators

Soft actuators can respond to fields (chemical, magnetic, electric) and convert the energy to mechanical deformation and have attracted significant attention in the bioengineering and energy storage fields. Stimuli that can actuate the deformation generally include pH, salt, light, heat, and electric and magnetic fields. In our review, we focused on applying 3D printing techniques in fabricating electroactive polymers, magnet-responsive polymers, and chemical-responsive polymers.

3.2.1. Electroactive Soft Actuators

Electroactive soft actuators (ESAs) were fabricated from electroactive polymers (EAPs) that can change shape or dimensions under electric fields. Based on their different actuation mechanisms, EAPs are usually categorized into two types: the electronic type and ionic type.

The electronic type generally includes (1) electrothermal actuators (ETAs) that can exhibit thermal expansion based on conductive composite sheets (carbon nanotube, graphene, conductive polymers) [115–120]; (2) dielectric elastomer actuators (DEAs) that comprise a thin polymer membrane (silicone, PU, acrylic elastomer) [118] sandwiched by two flexible electrodes and can deform under an electric field based on the Maxwell stress effect and electrostriction [114,115]; (3) liquid crystal elastomers (LCA) that have an intermediate state between a liquid phase and crystalline phase in polymers [121], deforming under electric fields based on the accumulation of mesogens reoriented from stretched conformation to random coil conformation [122]. This review will focus on applying 3D printing to DEAs due to their high efficiency, durability, and large actuation force.

The ionic type basically includes (1) ionic polymer actuators (IPAs) that can show fast and dual-oriented deformation in liquid under relatively low voltages (1–5 V) with alternating current based on volume-change mechanisms [123]; (2) ionic polymer–metal composite (IPMC) actuators that have an electrolyte-containing ionic polymer film sandwiched by two electrodes (Cu, Au, Pt, carbon, etc.), actuating under an electric field in dry conditions based on the accumulation of mobile ions on the electrolyte–electrode interface [119]; (3) Bucky gel actuators (BGAs) that have a three-layer structure with ionic liquids as electrolyte and a carbon source as electrodes, actuating in the air under an electric field based on changing C–C bond length and volume changes due to the large volume of ionic liquid molecules in pore structures of carbon-source electrodes [124]. This review mainly focuses on the 3D printing technology for IPAs due to the lack of 3D printing on IPMCs and BGAs owing to the complexity in assembly, despite providing good opportunities and large space in realizing three-layer configuration actuators that can work in air based on 3D printing techniques. Moreover, IPAs have attracted more interest due to their ease of control and manufacture, large response, actuation in wet conditions, and low voltage requirements.

Ionic Polymer Actuators

The expectation of an ideal IPA should include low activation voltage, rapid response time, large actuation force, good cycle stability, and high DOF. The most widely explored ionic polymers in actuator applications are commercial Nafion, Flemion, and Aquivion, which have ionic groups to exchange ions and perfluorinated backbones for supporting mechanical strength [125]. However, the 2D fabrication, complexity, and high cost of synthesizing these polymers limit their applications in designing the ideal IPA. Thus, many groups have demonstrated opportunities for 3D printing provided by DIW that can deposit ink and vat polymerization that can polymerize photocurable ink in solving these challenges [126]. To achieve fast and significant response (<5 s and 150°) as well as various motions, Wang et al. 3D-printed a jellyfish actuator using polyvinyl chloride (PVC) based ink with dibutyl adipate (DBA) as plasticizer based on the DIW technique, showing controlled movements under an electric field [87]. To decrease the actuation voltage (30 V) and achieve controlled manipulation (gripping and walking) with IPAs, Daehoon et al. introduced acrylic acid with carboxyl groups in the polymer backbone, increasing solvation and ion-exchange kinetics. The DLP-printed actuators can act as grippers constructed of bars with different thicknesses and walk in the salt solution like a human robot [127]. To further investigate the electroactive mechanisms and potential of other ionic gels, Yerin et al. synthesized sulfonyl group-containing hydrogels with acrylic acid and acrylamide. This work demonstrated good potential and fundamental knowledge in using the DLP method to study IPAs with different factors, including ionic strength, different types of ionic groups, crosslinking density, and voltage [128].

Dielectric Elastomer Actuators

The ideal DEA should have a high strain rate, large power density, fast response, and high actuation pressure [129]. The materials used in DEAs generally include PU-based, silicone-based, and acrylic elastomers that are traditionally fabricated by dip coating, spin coating, and solvent casting [130]. However, the restraint of DEA films requires using a rigid frame, limiting the design of actuator devices with complex geometries [131]. Moreover, the cyclability of contractile actuation can be impaired or broken due to the tearing of DEAs.

By increasing the cycle stability and achieving good actuation behavior, DIW techniques were applied to explore the potential of different printable inks to increase the performance of DE [132]. For instance, Daniela et al. merged the excellent properties of ionic liquid (IL) (high ionic conductivity, low vapor pressure, low viscosity, high thermal and electrochemical stability) and the electroactive response of poly(vinylidene fluoride) (PVDF) to produce IL/PVDF ink, DIW-printed by modifying the viscosity [133]. From a geometrical design perspective, some researchers have utilized inkjet printing to programmatically stack individual DE layers, achieving pre-stain-free performance without impairing the performance of DEA [134]. To provide a possible selection of materials, Alex et al. applied highly selective thiol-ene chemistry with step-growth polymerization in the curable ink for the DIW technique. The DEA based on poly(ethylene glycol ethylene sulfide) (PEG-PES) does not require restraint due to the interdigitated vertical design by DIW printing. Moreover, self-healing properties were achieved with tunable mechanical properties by modifying the viscosity of curable inks [88].

3.2.2. Magnetically Responsive Soft Actuator

Magnetic materials can respond to a magnetic field, and are generally categorized into four types listed according to their magnetic strength: ferromagnetic > diamagnetic > paramagnetic > antimagnetic [123]. A magnetically responsive soft actuator (MSA) can show fast response, large force, and remote control under a magnetic field. Strongly ferromagnetic nanoparticles (FNPs), such as magnetite (Fe_3O_4) or neodymium-ion-boron (NdFeB), can stabilize in liquid phase by coating surfactant to form magnetic fluid, absorbed into polymer gels [92]. FNPs can be immobilized in the gel network by forming physical crosslinking between Fe(III) or Fe(II) and ligands of polymer, showing good potential for applications in release control, encapsulation for display devices, and drug delivery [135].

DIW and FFF techniques have been widely used to print MSAs with ink or thermoplastic with a high load of magnetic fillers [89,130]. For instance, Bastola et al. 3D-printed a magnetorheological elastomer by modifying the optimum rheology of silicone/carbonyl iron particle solutions based on the DIW technique. However, some drawbacks limit the application of DIW and FFF in printing MSAs: (1) the resolution of samples printed by extruding filaments is low; (2) the inhomogeneous segregation of magnetic nanoparticles in the dispersion can result in heterogeneous MSA response. Thus, the DLP technique that can polymerize low-viscous (<5 Pa·s) photocurable ink can provide higher product resolutions and ease of manufacturing. The challenges of the DLP technique are to understand the effect of magnetic fillers in photopolymerization and viscosity barriers due to the high loading of fillers, resulting in macroscopic sedimentation in photocurable ink. To understand the photopolymerization of photocurable ink with magnetic fillers and print MSAs with optimized reactivity and mechanical properties, Simone et al. fabricated a programmable MSA based on the DLP technique by blending six wt% magnetite nanoparticles and urethane-acrylate resins with butyl acrylate as a reactive diluent [89]. Zhongying et al. DLP-printed a flexible 2-arm gripper by synthesizing an ink that contained Fe_3O_4 nanoparticles, polyethylene glycol, 2-[(butylcarbomoyl)oxy]ethyl acrylate, and cyclic trimethylolpropane formal acrylate as reactive diluents, where the final products showed excellent printing quality and mechanical properties [136].

3.2.3. Chemically Responsive Soft Actuators

Chemically responsive soft actuators (CSAs) can deform under stimuli including pH, salt, solvents, and temperature, by changing their volume or shape due to the swelling/shrinking process based on polymer–solvent interaction mechanisms such as Flory–Rehner [137], Donnan's theory [138], or hydrodynamic models [139]. The typical materials for CSAs are hydrogels that have a 3-dimensional (3D) crosslinked polymer network, incorporating a tremendous amount of solution. The prevalent CSA-based hydrogel actuators are synthesized from polymer hosts such as polyacrylic acid (PAA), polyvinyl alcohol (PVA), poly (acrylamide) (PAAm), poly (*N*-isopropyl acrylamide) (PNIPAM), and poly (2-acrylamido-2-methylpropane sulfonic acid) (PAMPS) [126]. These polymers can be easily polymerized with the free-radical polymerization (FRP) method due to the presence of double bonds in precursor monomers, which is also widely used in vat polymerization 3D printing (VPP) techniques (DLP, SLA, CLIP). Thus, most research has been focused on exploring the applications of VPP in designing CSAs.

For instance, Odent et al. designed a multi-responsive (solvent, pH, temperature) hydrogel actuator with high resolution and gradient-like structures based on the SLA technique [93]. This hydrogel actuator demonstrated the controllability of bionic actuators under various environmental changes [93]. Sujan et al. demonstrated a dual-responsive (pH and temperature) hydrogel actuator, based on photocurable ink comprising F127 dimethacrylate (FdMA) and acrylic acid comonomers, using the SLA technique [140]. The 3D printed valve and dual slab actuators showed controlled locomotion under changes in temperature (6 °C to 37 °C) and pH (2 to 7.4) [140].

By adjusting the rheology of polymer suspensions to achieve better printability, many works have tried to fabricate extruded inks for DIW and inkjet techniques. Yuan et al. synthesized a novel ink composed of poly(ethylene glycol), diacrylate (PEGDA), and polyethyleneimine-co-poly(acrylic acid) (PEI-*co*-PAA) copolymer, printing actuators responsive to humidity and solvents based on the DIW technique [90]. The printed soft gripper can provide 0.2 N force, softly catching goldfish without harm [90]. Chang et al. fabricated an Fe^{3+} reinforced hydrogel actuator that incorporates Dulbecco's Modified Eagle Medium and egg white, a significant nutrition source, based on the DIW technique [141]. Shannon et al. fabricated a temperature-responsive hydrogel actuator based on ink that has alginate/PNIPAM with the DIW technique [142]. The actuator showed a reversible volume change at a critical temperature (about 32–35 °C) due to the coil–globule transition in the polymer network [142].

3.3. Flexible Electronics

Flexible electronics (FEs) are of growing interest for applications including smartphones, wearable devices, and portable displays [143]. Ideally, FEs should be soft, portable, wearable, biocompatible, have considerable mechanical strength and geometrical stability, and be adaptive to dynamic surfaces [144]. To facilitate the evolution of high-performance FEs, advanced manufacturing techniques for intelligent materials have been widely explored. The following discusses recent literature on the fabrication of sensors and energy-storage devices, emphasizing the optimization of 3D printing techniques in materials and designs as summarized in Figure 5.

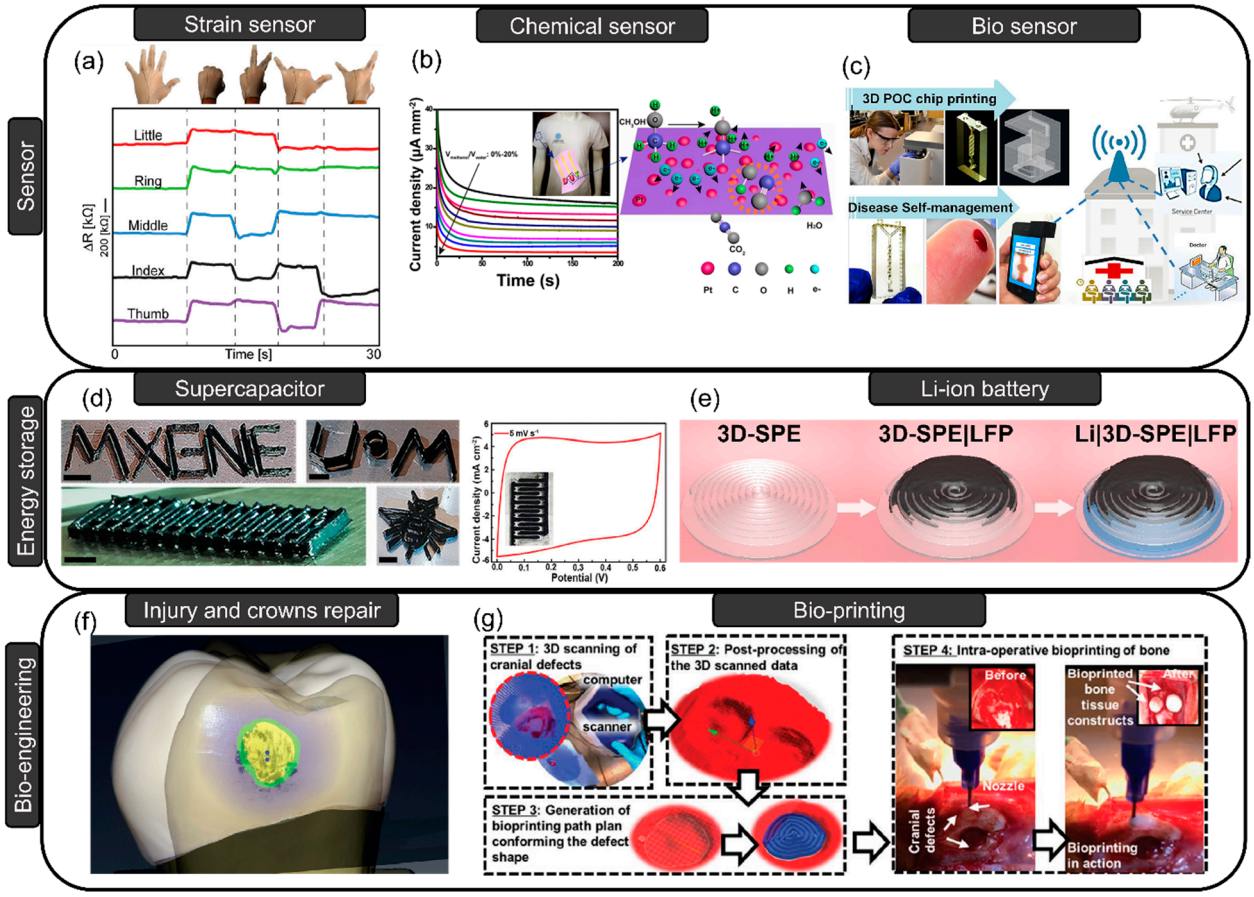

Figure 5. (**a**) DIW-printed wearable strain sensor. Adapted with permission from Ref. [145]. Copyright 2022 John Wiley and Sons. (**b**) Screen-printed methanol gas sensor. Adapted with permission from Ref. [146]. Copyright 2019 American Chemical Society. (**c**) 3D-printed point-of-care (POC) microfluidic chip that rapidly (60 s) diagnoses anemia via smartphones. Adapted with permission from Ref. [147]. Copyright 2022 AIP Publishing. (**d**) DIW-printed MXene architectures for supercapacitors. Adapted with permission from Ref. [148]. Copyright 2022 John Wiley and Sons. (**e**) SLA-printed polymer electrolyte for Li-ion battery. Adapted with permission from Ref. [101]. Copyright 2020 American Chemical Society. (**f**) Inkjet printing to fit interim crowns of teeth. Adapted with permission from Ref. [149]. Copyright 2022 Elsevier. (**g**) Bioprinting tissues based on 3D scanning for rat surgery Ref. [150]. Copyright 2022 John Wiley and Sons.

3.3.1. Sensors

Flexible sensors (FSs) can respond to environmental stimulation, generating readable signals. The stimulation is generally of three types (physical, chemical, and biological) based on various responsive mechanisms. Physical FSs can respond to temperature, humidity, pressure, and light [151]. Chemical FSs can capture chemical signals from sources such as gas, solvents, ions, and body fluids (blood, urine, sweat, etc.). Bio-FSs can recognize or react with biological matter, including DNA, RNA, viruses, antibodies, proteins, etc. [152]. To achieve highly compatible human–device interactions, FSs are strongly dependent on more-customized manufacturing methods (3D printing). For instance, Joseph et al. utilized the DIW technique to print a strain sensor with high elasticity and conformability to dimensional shape change, eliminating the delamination in the interfaces between each layer by writing the ink in an elastomeric reservoir [145].

Traditional physical sensors composed of rigid substrates (glass or silica) have been used in many applications in human healthcare, electronic devices, and wearable monitoring devices. Flexibility is the key, and the most significant obstacles to developing physical FSs are surmounted by using flexible substrate materials to achieve perfect human–

device interactions. Many efforts have combined elastomer elasticity and the sensing ability of conductive fillers by synthesizing a flexible composite sensor [148,149]. However, the resistance of physical FSs can still change due to external strain or loose interfacial contact, impairing the accuracy and reliability of output data. To solve the challenge, a long-range ordered cellular framework was recently reported to improve the stability of electric conductivity by sharing the external strains [153–155]. Three-dimensional printing techniques have exhibited great potential in printing these types of complex structures with high resolutions. For instance, Wang et al. utilized the DIW technique to print a temperature sensor with cellular structures (grid, triangle-porous, hexagonal-porous) based on graphene/PDMS composites, showing reliable and stable measurements under various loading modes [95]. Xiao et al. demonstrated the DLP method in printing strain sensor arrays based on multiwalled carbon nanotube (MWCNT)/poly (epoxy aliphatic acrylate-*co*-aliphatic urethane diacrylate) (PEAA-*co*-AUD) composites, combined with a near-field communication (NFC) circuit and showing high sensitivity and strain detection range [156]. Moreover, the FFF technique has been applied to humidity sensors based on acrylonitrile butadiene styrene (ABS)/boron-doped diamond (BDD)/LiCl composite filaments due to the minimum shrinkage of final printed samples, opening a vast space for extruded thermoplastic/filler composites [96].

Chemical and bio sensors that can detect chemicals have exhibited great potential in air pollution detection, human body monitoring, and bioengineering. Chemical sensors have sensing mechanisms similar to those of biosensors. Flexible chemical and bio sensors also rely on 3D printing techniques to print flexible substrate/filler composites. Wu et al. demonstrated a gas sensor that can detect methanol vapor by alcoholysis of boron/oxygen dative bonds in methanol based on FFF by synthesizing extruded filaments from polyborosiloxane (PBS)/graphene rod composites with self-healing properties [157]. FFF, SLA, Polyjet, SLS, Inkjet, and DLA have all been utilized for manufacturing bio FSs with the advantages and disadvantages summarized elsewhere [158].

3.3.2. Batteries and Supercapacitors

Lithium-ion batteries (LIBs) have been one of the most important energy sources for many applications in portable devices, including smartphones, electronic watches, desktops, etc. However, safety issues due to lithium dendrite growth have caused some disasters, such as exploding Samsung mobile phones and fires in Tesla electric cars [159]. Recent research has sought solutions to this challenge by utilizing solid-state LIBs where the typical liquid electrolyte is replaced by a solid electrolyte, including organic, inorganic, and composite types [160]. However, inorganic solid electrolytes (ISEs), such as ceramic $Li_7La_3Zr_2O_{12}$ (LLZ-type), have rather low wettability, resulting in poor interfacial contact, increasing the resistance significantly [161]. To address the challenge of poor contact, new geometries that can increase the contact areas between electrode/electrolyte interfaces have been developed. Three-D printing is a candidate for producing special-shape structures at wide-length scales to investigate the interfacial structure–property relationships in LIBs. For instance, Dennis et al. demonstrated the first DIW-printed ceramic solid electrolyte (LLZ-type) with a stacked array and "log-cabin" type structures, realizing safer, stable, and high-energy-density LIBs [100]. Moreover, the DIW technique has also been applied in printing both anodes and cathodes [162]. Polymer electrolytes that can store solutions, ions, and conduct ions have emerged, offering great potential in realizing solid-state LIBs due to advantages, including good flexibility, high ionic conductivity, excellent contact and wettability with electrodes, high lithium transference number, and decent thermal and electrochemical stability [163]. He et al. demonstrated an SLA-printed polymer electrolyte for assembling LIBs based on PEGDA and poly(ethylene oxide) (PEO), showing high ionic conductivity (3.7×10^{-4} S cm^{-1} at room temperature), increased lithium salt loading, good retention, and low interfacial impedance [101]. Digital printing techniques have also been applied in fabricating solid polymer electrolytes to design particular configurations, increasing polymer electrolyte performance [164]. However, vat polymerization

methods typically only print polymers, such that the ultimate assembly of an entire battery device with complex geometry remains a challenge. FFF multi-material printing has excellent potential in overcoming this challenge to realize fully printed batteries. For instance, Alexis et al. demonstrated the first fully printed solid-state battery based on PEO/lithium bis(trifluoromethanesulfonyl)imide (LiTFSI), showing good ionic conductivity (2.18×10^{-3} S cm^{-1} at 90 °C) [165].

Supercapacitors with high safety and high power density have been candidates for replacement of batteries or as complementary energy sources [80]. However, the leakage of hazardous liquid electrolytes and self-discharging have limited the practical applications of supercapacitors. Flexible supercapacitors (FSCs), generally composed of a polymer separator sandwiched by two electrodes, can solve this challenge. Some of the 3D printing techniques have been focused on electrodes, with some others on polymer electrolytes. For instance, Yang et al. demonstrated free-standing MXene electrodes that were fabricated by the DIW technique, realizing large capacitance (245 F g^{-1} at 0.2 A g^{-1}) and decent retention (90% after 10,000 cycles) [148]. Shen et al. utilized the Inkjet technique to print semi-solid state micro-supercapacitors based on polyvinyl alcohol (PVA)/ LiCl ink and achieved large areal capacitance (207.9 mF cm^{-2}) [98]. Moreover, the 3D paste printing method provides an excellent opportunity to achieve fully printed FSCs by changing syringes with multi-materials [166]. Milad et al. prepared an electrical double-layer capacitor (EDLC) based on the 3D paste printing technique, printing the activated carbon electrode, PVA gel electrolyte, and silver-based current collector simultaneously [167].

4. Bioengineering

Bioengineering aims to manufacture biomedical devices and implants, such as orthopedic implants, prostheses, orthoses, dental implants, anatomical models, and many other surgical apparatuses that are compatible with the patient's anatomy [168,169]. Challenges for these biomedical instruments include demands for rigidity and unique configurations for each patient. Three-D printing techniques that can fabricate complex parts with high-resolution detail and controlled material properties offer a solution by printing more flexible and lighter products [162,163]. The following reviews the application of 3D printing techniques in addressing these challenges for biomedical instruments.

Physical surgeries, including dental and maxillofacial surgery, as well as prosthetics and orthopedic surgery can correct facial defects, repair the functions of missing limbs, and fix fractured bones, respectively. Customized designs of 3D-printed prototypes can fit nicely in injured parts, improving the quality of life of patients. Computer-aided manufacturing (CAM) systems can be utilized to identify virtual imperfections through scanning to address trauma and periodontal disease due to the incompatibility of implants. For instance, Werz et al. simulated human jaws with FFF techniques based on silicon rubber and thermoplastic polymers [170]. Computed tomography (CT) has also been applied to collect images of fractured clavicles in patients undergoing minimally invasive plate osteosynthesis (MIPO) procedures [171]. The fracture locations depend on the particular clavicle fractures, and physicians rely on building 3D models to perform the surgery [171]. Moreover, 4D printing that can print shape-memory materials based on 3D printing techniques has been utilized to fabricate prostheses with pneumatic actuators and soft sensors as moving fingers [172].

Patients suffering from organ impairment need replacement organs to restore their health when their condition is significantly severe. The ultimate goal in this case is to grow autologous tissue for future replacements [173]. Bioprinters can print biomaterials with organ-like structures using materials that incorporate living cells, which subsequently multiply and grow in the designed geometry. In this case, the bioprinting technique offers good opportunities for tissue engineering, transplantation, drug screening, and cancer treatments by generating hepatorganoids with biocompatible materials and living cells [174]. Xie et al. utilized bioprinting to build hepatorganoids for treating hepatocellular carcinoma (HCC) by generating cell line models and performing drug screening. However,

bioprinting still has a long way to go before mass production. The major challenge is that suitable environments for cells require in vivo vascularization for the supply of oxygen and nutrition and removal of waste [175].

5. Earth Sciences

Researchers in the geosciences have been using additive manufacturing to fabricate porous media replicating the physical, hydraulic, mechanical and chemical properties of natural samples. A wide variety of materials, including filaments, thermoplastics, polymers, photosensitive epoxy resins, etc., and printing methods have been explored to fabricate complex porous structures [176]. Creating the digital model, which is the first step in any 3D printing project, can be based either on the design of an ideal porous media system or one extracted from real samples. In the first approach, a simple fracture network or porous structure is designed in computer-aided design (CAD) software such as AutoCAD, OpenSCAD, etc. [177], or an artificial digital porous model is built by distributing 3D shapes (commonly spheres and cylinders) in a given volume based on a prescribed algorithm [178,179]. These models are then converted into an object file that can be read by the printing software. This approach provides the freedom to create various shapes and structures to fit the desired experimental requirements. On the other hand, non-destructive, advanced imaging tools can be utilized to capture macro and micropores from undisturbed soil [180,181], sandstone [182,183], or shale [184,185] samples. Nowadays, high-performance computers and advanced imaging tools such as 3D X-ray computed tomography (X-ray CT) can reconstruct 3D models of the pore geometries of natural samples at high resolution (microns). The 3D images can be segmented and further processed to create a 3D mesh for printing. After printing and post-processing, the printed samples can be imaged again in 3D to extract various properties.

The quality of the printed specimens can vary with the printing approach and material, even between replicates. Comparing binder jetting, fused filament fabrication (FFF) and stereolithography apparatus (SLA) methods, Almetwally and Jabbari observed that samples printed with a gypsum-based ProJet printer with binder jetting technology had porosity and permeability closest to that of the real sandstone sample [186]. In a later study, they observed that SLA 3D printing also provides precise porosity and permeability [177]. It should be noted, however, that some studies have observed a lower porosity in SLA-printed specimens compared to the original samples due to the trapping of residual resin in micropores [187,188]. Post-processing steps, such as pressurized flushing with ethanol, have been shown to improve porosities for SLA-printed replicas of sedimentary rock [187]. Kong et al. employed a binder jetting printing system with silica sand as the base material to study the microstructure in sandstone samples [189]. They observed a variation in porosity in the printed sample compared to the real Berea sandstone sample; however, the pore size distribution of the printed sample agreed well with the real sample.

Three-D printing has also shown utility in the investigation of hydraulic properties of soil samples where experiments can be challenging due to alteration of internal pore structures. Bacher et al. explored the use of four different 3D printing techniques: fused filament fabrication (FFF), selective laser sintering (SLS), PolyJet and stereolithography apparatus (SLA) to replicate macropore networks in undisturbed soil samples for water and solute transport experiments [180]. They used acrylonitrile-butadiene-styrene (ABS), alumide, polyamide, high-detail resin, and prime gray epoxy resin as printing materials and measured the hydraulic conductivity of the printed samples using the constant head method [180]. Out of the five materials, the specimen printed using the prime gray epoxy resin material was free of residual clogging and hence had the largest and most similar hydraulic conductivity to that of the original undisturbed soil sample [180]. They also noted that the SLS technique is prone to micropore clogging by the residual unsolidified printing material, which needs to be removed by mechanical means [180]. Hence, this method is unsuitable for investigating hydraulic and solute transport properties unless the clogging issue is resolved [180]. Dal Ferro and Morari performed a similar study aiming to fabricate

porous media reflecting the hydraulic conductivity of soil samples utilizing the MultiJet 3D printing technology with resin containing an organic mixture as the printing material [181]. The resulting printed prototype had one order of magnitude higher saturated hydraulic conductivity compared to the undisturbed soil sample. The observed higher hydraulic conductivity likely resulted from microstructure printing limitations, where Ishutov et al. noted that a minimum pore throat diameter of 400 µm could be printed accurately with stereolithography 3D printing technology [187].

The macroscopic response of hydraulic properties due to changes in pore network structure can also be investigated by manipulating printing mesh of porous media. Head and Vanorio successfully tested two different 3D printers, a stereolithography desktop printer and MultiJet industrial printer, to explore the ability to manipulate printed microstructures and measure the changes in flow properties [190]. For both printers, they used photosensitive resin as the printing material [190]. They downscaled a vertically connected pore structure in a carbonate sample to mimic the pore volume compaction and observed a decreasing trend in measured and simulated permeability with decreasing porosity [190]. However, for the dissolution model, they enlarged the pore throat diameter without changing the overall length and noted a dramatic change in permeability for a minor change in porosity [190].

Additive manufacturing has also shown utility for investigating rock mechanics. Jiang and Zhao studied the unconfined compressive strength (UCS) and direct tensile strength (DTS) of specimens with different shapes and structures printed by FFF using PLA [191]. Their study found that under compression, the specimen exhibited more ductile behavior, and in tensile strength tests, it tended to be more brittle [191]. Stress–strain behavior of printed samples similar to that of natural rock samples as measured with the mechanical compressive strength test was noted in by Jiang et al., who used a ProJet printer with sand powder and binder material [192]. Moreover, the crack propagation also agreed well with the fracturing behavior of real rock samples under compression. The binder material plays a critical role in the UCS of printed specimens as noted in Hodder et al. for sandstone samples fabricated using an M-Flex sand printer with silica sand coated with p-toluene sulphonic acid (activator) as the base material [193]. Upon addition of the binder material (main component: furfuryl alcohol), a condensation reaction took place, creating polymer necks between the solid grains [193]. UCS tests conducted on the cylindrical replicas showed an increase in the UCS with a higher amount of binder material; however, above 8 vol%, they saw instability as the binder material started to clog the pore network and fracture [193].

Printing porous media with geochemically reactive properties was first explored by Anjikar et al. as a means to enhance understanding of geochemical reactions in porous media [182]. They replicated a sandstone sample with the FFF using novel reactive filaments fabricated by combining high-impact polystyrene and calcite in varying amounts [182]. Three-D images of the printed specimens revealed that the amount of calcite in the printed sample agreed well with the amount mixed with filament; however, the normalized calcite surface area in the printed sample was an order of magnitude lower than real samples containing similar amounts of calcite. The resulting accessible calcite surface areas, however, agreed well with those determined for real sandstone samples in the literature, suggesting this is a promising means of creating reactive porous media specimens [182].

6. Summary and Conclusions

Polymer composites are important materials in industrial and consumer applications. From recent investigations, such as those discussed herein, it is evident that the potential scope of 3D printing of multifunctional materials for different industrial and scientific applications is enormous. The different additive manufacturing technologies have found application for the fabrication of prototypes and customized parts for aerospace, automobile, electronics, and biomedical applications, and the use of 3D printing in manufacturing is expected to increase as materials and methods improve. This review paper discussed

different polymer materials and research studies aimed at improving material chemistry, morphology, and processing for 3D printing of multi-functional systems and the practical utility of additive manufacturing technologies at commercial scale. However, many challenges remain, for example, in terms of repeatability and consistency in the manufactured parts and comparative analysis with standard products based on accuracy, sustainability, and product shelf life. Studies based on smart multi-functional material manufacturing to construct electronic devices, biomatrices, and energy storage devices have laid the foundation for the increased application of 3D printing in these areas. Nonetheless, additional work on material development, process development and control, testing and certification of 3D printed parts will be needed to bring the full potential of 3D printing to bear towards improving conditions for humanity and planet Earth.

Author Contributions: Conceptualization, V.V.S., Y.W. and B.S.B.; writing—original draft preparation, V.V.S., Y.W., M.F.S., L.E.B. and B.S.B.; writing—review and editing, V.V.S., Y.W., M.F.S., M.L.A., L.E.B. and B.S.B.; funding acquisition, M.L.A., L.E.B. and B.S.B. All authors have read and agreed to the published version of the manuscript.

Funding: This material is based upon work supported by the National Science Foundation under Grant No. 2025626. Y.W. and M.L.A. acknowledge support for this work by the Auburn University Center for Polymers and Advanced Composites.

Institutional Review Board Statement: Not applicable.

Informed Consent Statement: Not applicable.

Data Availability Statement: No new data were created or analyzed in this study. Data sharing is not applicable to this article.

Conflicts of Interest: The authors declare no conflict of interest.

References

1. Zindani, D.; Kumar, K. An insight into additive manufacturing of fiber reinforced polymer composite. *Int. J. Lightweight Mater. Manuf.* **2019**, *2*, 267–278. [CrossRef]
2. Parandoush, P.; Lin, D. A review on additive manufacturing of polymer-fiber composites. *Compos. Struct.* **2017**, *182*, 36–53. [CrossRef]
3. Mohr, S.; Khan, O. 3D Printing and the Future of Supply Chains. In *Proceedings of the Hamburg International Conference of Logistics (HICL)*; epubli GmbH: Berlin, Germany, 2015. Available online: http://www.dhl.com/content/dam/downloads/g0/about_us/logistics_insights/dhl_trendreport_3dprinting.pdf (accessed on 21 January 2022).
4. Kumar, S.; Kruth, J.-P. Composites by rapid prototyping technology. *Mater. Des.* **2009**, *31*, 850–856. [CrossRef]
5. Razavykia, A.; Brusa, E.; Delprete, C.; Yavari, R. An Overview of Additive Manufacturing Technologies—A Review to Technical Synthesis in Numerical Study of Selective Laser Melting. *Materials* **2020**, *13*, 3895. [CrossRef] [PubMed]
6. Goodridge, R.; Shofner, M.; Hague, R.; McClelland, M.; Schlea, M.; Johnson, R.; Tuck, C. Processing of a Polyamide-12/carbon nanofibre composite by laser sintering. *Polym. Test.* **2011**, *30*, 94–100. [CrossRef]
7. Cheah, C.; Fuh, J.; Nee, A.; Lu, L. Mechanical characteristics of fiber-filled photo-polymer used in stereolithography. *Rapid Prototyp. J.* **1999**, *5*, 112–119. [CrossRef]
8. Chiu, S.-H.; Wicaksono, S.T.; Chen, K.-T.; Chen, C.-Y.; Pong, S.-H. Mechanical and thermal properties of photopolymer/CB (carbon black) nanocomposite for rapid prototyping. *Rapid Prototyp. J.* **2015**, *21*, 262–269. [CrossRef]
9. Sakly, A.; Kenzari, S.; Bonina, D.; Corbel, S.; Fournée, V. A novel quasicrystal-resin composite for stereolithography. *Mater. Des.* **2014**, *56*, 280–285. [CrossRef]
10. Gurr, M.; Hofmann, D.; Ehm, M.; Thomann, Y.; Kübler, R.; Mülhaupt, R. Acrylic Nanocomposite Resins for Use in Stereolithography and Structural Light Modulation Based Rapid Prototyping and Rapid Manufacturing Technologies. *Adv. Funct. Mater.* **2008**, *18*, 2390–2397. [CrossRef]
11. Kim, J.H.; Lee, S.; Wajahat, M.; Jeong, H.; Chang, W.S.; Jeong, H.J.; Yang, J.-R.; Kim, J.T.; Seol, S.K. Three-Dimensional Printing of Highly Conductive Carbon Nanotube Microarchitectures with Fluid Ink. *ACS Nano* **2016**, *10*, 8879–8887. [CrossRef]
12. El Moumen, A.; Tarfaoui, M.; Lafdi, K. Additive manufacturing of polymer composites: Processing and modeling approaches. *Compos. Part B Eng.* **2019**, *171*, 166–182. [CrossRef]
13. Perelaer, J.; Smith, P.J.; Mager, D.; Soltman, D.; Volkman, S.K.; Subramanian, V.; Korvink, J.G.; Schubert, U.S. Printed electronics: The challenges involved in printing devices, interconnects, and contacts based on inorganic materials. *J. Mater. Chem.* **2010**, *20*, 8446–8453. [CrossRef]

14. Seerden, K.A.M.; Reis, N.; Evans, J.R.G.; Grant, P.S.; Halloran, J.W.; Derby, B. Ink-Jet Printing of Wax-Based Alumina Suspensions. *J. Am. Ceram. Soc.* **2001**, *84*, 2514–2520. [CrossRef]
15. Masood, S.H.; Song, W.Q. Development of new metal/polymer materials for rapid tooling using Fused deposition modelling. *Mater. Des.* **2004**, *25*, 587–594. [CrossRef]
16. Plymill, A.; Minneci, R.; Greeley, D.A. TRACE: Tennessee Research and Creative Graphene and Carbon Nanotube PLA Composite Feedstock Development for Fused Deposition Modeling Graphene and Carbon Nanotube PLA Composite Feedstock Development for Fused Deposition Modeling, 2016. Chancellor's Honors Program Projects. 1955. Available online: https://trace.tennessee.edu/utk_chanhonoproj/1955 (accessed on 21 January 2022).
17. Nikzad, M.; Masood, S.; Sbarski, I. Thermo-mechanical properties of a highly filled polymeric composites for Fused Deposition Modeling. *Mater. Des.* **2011**, *32*, 3448–3456. [CrossRef]
18. Carneiro, O.S.; Silva, A.F.; Gomes, R. Fused deposition modeling with polypropylene. *Mater. Des.* **2015**, *83*, 768–776. [CrossRef]
19. Milosevic, M.; Stoof, D.; Pickering, K.L. Characterizing the Mechanical Properties of Fused Deposition Modelling Natural Fiber Recycled Polypropylene Composites. *J. Compos. Sci.* **2017**, *1*, 7. [CrossRef]
20. Mwema, F.M.; Akinlabi, E.T. Basics of Fused Deposition Modelling (FDM). In *SpringerBriefs in Applied Sciences and Technology*; Springer: Berlin, Germany, 2020.
21. Ahn, D.; Kweon, J.-H.; Kwon, S.; Song, J.; Lee, S. Representation of surface roughness in fused deposition modeling. *J. Mater. Process. Technol.* **2009**, *209*, 5593–5600. [CrossRef]
22. Wang, P.; Zou, B.; Ding, S.; Li, L.; Huang, C. Effects of FDM-3D printing parameters on mechanical properties and microstructure of CF/PEEK and GF/PEEK. *Chin. J. Aeronaut.* **2020**, *34*, 236–246. [CrossRef]
23. Dickson, A.N.; Abourayana, H.M.; Dowling, D.P. 3D Printing of Fibre-Reinforced Thermoplastic Composites Using Fused Filament Fabrication—A Review. *Polymers* **2020**, *12*, 2188. [CrossRef]
24. Ning, F.; Cong, W.; Qiu, J.; Wei, J.; Wang, S. Additive manufacturing of carbon fiber reinforced thermoplastic composites using fused deposition modeling. *Compos. Part B Eng.* **2015**, *80*, 369–378. [CrossRef]
25. Ferreira, R.T.L.; Amatte, I.C.; Dutra, T.A.; Bürger, D. Experimental characterization and micrography of 3D printed PLA and PLA reinforced with short carbon fibers. *Compos. Part B Eng.* **2017**, *124*, 88–100. [CrossRef]
26. Yao, X.; Luan, C.; Zhang, D.; Lan, L.; Fu, J. Evaluation of carbon fiber-embedded 3D printed structures for strengthening and structural-health monitoring. *Mater. Des.* **2017**, *114*, 424–432. [CrossRef]
27. Ramalingam, P.S.; Mayandi, K.; Balasubramanian, V.; Chandrasekar, K.; Stalany, V.M.; Munaf, A.A. Effect of 3D printing process parameters on the impact strength of onyx—Glass fiber reinforced composites. *Mater. Today Proc.* **2020**, *45*, 6154–6159. [CrossRef]
28. Nuñez, P.; Rivas, A.; García-Plaza, E.; Beamud, E.; Sanz-Lobera, A. Dimensional and Surface Texture Characterization in Fused Deposition Modelling (FDM) with ABS plus. *Procedia Eng.* **2015**, *132*, 856–863. [CrossRef]
29. Yasa, E.; Ersoy, K. Dimensional Accuracy and Mechanical Properties of Chopped Carbon Reinforced Polymers Produced by Material Extrusion Additive Manufacturing. *Materials* **2019**, *12*, 3885. [CrossRef]
30. Rybachuk, M.; Mauger, C.A.; Fiedler, T.; Öchsner, A. Anisotropic mechanical properties of fused deposition modeled parts fabricated by using acrylonitrile butadiene styrene polymer. *J. Polym. Eng.* **2017**, *37*, 699–706. [CrossRef]
31. Yunus, D.E.; He, R.; Shi, W.; Kaya, O.; Liu, Y. Short fiber reinforced 3d printed ceramic composite with shear induced alignment. *Ceram. Int.* **2017**, *43*, 11766–11772. [CrossRef]
32. Bond, I.; Trask, R.; Williams, H.R. Self-Healing Fiber-Reinforced Polymer Composites. *MRS Bull.* **2008**, *33*, 770–774. [CrossRef]
33. Blaiszik, B.; Kramer, S.; Olugebefola, S.; Moore, J.; Sottos, N.; White, S. Self-Healing Polymers and Composites. *Annu. Rev. Mater. Sci.* **2010**, *40*, 179–211. [CrossRef]
34. Xu, H.; Tang, Y.; Liu, Z.; Cai, Y.; Wang, Y. The study of typical failure modes and failure mechanism of polymer materials. *IOP Conf. Ser. Mater. Sci. Eng.* **2017**, *231*, 12123. [CrossRef]
35. Kim, C.; Ejima, H.; Yoshie, N. Polymers with autonomous self-healing ability and remarkable reprocessability under ambient humidity conditions. *J. Mater. Chem. A* **2018**, *6*, 19643–19652. [CrossRef]
36. Terryn, S.; Mathijssen, G.; Brancart, J.; Lefeber, D.; Van Assche, G.; Vanderborght, B. Development of a self-healing soft pneumatic actuator: A first concept. *Bioinspir. Biomim.* **2015**, *10*, 046007. [CrossRef] [PubMed]
37. White, S.R.; Sottos, N.R.; Geubelle, P.H.; Moore, J.S.; Kessler, M.R.; Sriram, S.R.; Brown, E.N.; Viswanathan, S. Autonomic healing of polymer composites. *Nature* **2001**, *409*, 794–797. [CrossRef] [PubMed]
38. Zhai, L.; Narkar, A.; Ahn, K. Self-healing polymers with nanomaterials and nanostructures. *Nano Today* **2019**, *30*, 100826. [CrossRef]
39. Chen, X.; Dam, M.A.; Ono, K.; Mal, A.; Shen, H.; Nutt, S.R.; Sheran, K.; Wudl, F. A Thermally Re-mendable Cross-Linked Polymeric Material. *Science* **2002**, *295*, 1698–1702. [CrossRef] [PubMed]
40. Chen, X.; Wudl, F.; Mal, A.K.; Shen, H.; Nutt, S.R. New Thermally Remendable Highly Cross-Linked Polymeric Materials. *Macromolecules* **2003**, *36*, 1802–1807. [CrossRef]
41. Hong, G.; Zhang, H.; Lin, Y.; Chen, Y.; Xu, Y.; Weng, W.; Xia, H. Mechanoresponsive Healable Metallosupramolecular Polymers. *Macromolecules* **2013**, *46*, 8649–8656. [CrossRef]
42. Peterson, A.M.; Jensen, R.E.; Palmese, G.R. Room-Temperature Healing of a Thermosetting Polymer Using the Diels−Alder Reaction. *ACS Appl. Mater. Interfaces* **2010**, *2*, 1141–1149. [CrossRef]

43. Zeng, C.; Seino, H.; Ren, J.; Hatanaka, K.; Yoshie, N. Bio-Based Furan Polymers with Self-Healing Ability. *Macromolecules* **2013**, *46*, 1794–1802. [CrossRef]
44. Xie, M.; Che, Y.; Liu, K.; Jiang, L.; Xu, L.; Xue, R.; Drechsler, M.; Huang, J.; Tang, B.Z.; Yan, Y. Plastic Supramolecular Films: Caking-Inspired Cold Sintering of Plastic Supramolecular Films as Multifunctional Platforms. *Adv. Funct. Mater.* **2018**, *28*, 36. [CrossRef]
45. Ghosh, B.; Urban, M.W. Self-Repairing Oxetane-Substituted Chitosan Polyurethane Networks. *Science* **2009**, *323*, 1458–1460. [CrossRef] [PubMed]
46. Scheiner, M.; Dickens, T.J.; Okoli, O. Progress towards self-healing polymers for composite structural applications. *Polymer* **2016**, *83*, 260–282. [CrossRef]
47. Kessler, M.; White, S. Self-activated healing of delamination damage in woven composites. *Compos. Part A Appl. Sci. Manuf.* **2001**, *32*, 683–699. [CrossRef]
48. Kessler, M.; Sottos, N.; White, S. Self-healing structural composite materials. *Compos. Part A Appl. Sci. Manuf.* **2003**, *34*, 743–753. [CrossRef]
49. Shinde, V.V.; Celestine, A.-D.; Beckingham, L.E.; Beckingham, B.S. Stereolithography 3D Printing of Microcapsule Catalyst-Based Self-Healing Composites. *ACS Appl. Polym. Mater.* **2020**, *2*, 5048–5057. [CrossRef]
50. Shinde, V.V.; Shelke, S.D.; Celestine, A.N.; Beckingham, B.S. Self-healing in high impact polystyrene (HIPS) composites via embedded non-toxic solvent-filled microcapsules. *J. Appl. Polym. Sci.* **2021**, *139*, 51463. [CrossRef]
51. Garcia, S.J.; Fischer, H.R. Self-healing polymer systems: Properties, synthesis and applications. In *Smart Polymers and their Applications*; Woodhead Publishing: Cambridge, UK, 2014.
52. Plaisted, T.A.; Nemat-Nasser, S. Quantitative evaluation of fracture, healing and re-healing of a reversibly cross-linked polymer. *Acta Mater.* **2007**, *55*, 5684–5696. [CrossRef]
53. Fischer, H. Self-repairing material systems—A dream or a reality? *Nat. Sci.* **2010**, *2*, 873–901. [CrossRef]
54. Park, J.S.; Takahashi, K.; Guo, Z.; Wang, Y.; Bolanos, E.; Hamann-Schaffner, C.; Murphy, E.; Wudl, F.; Hahn, H.T. Towards Development of a Self-Healing Composite using a Mendable Polymer and Resistive Heating. *J. Compos. Mater.* **2008**, *42*, 2869–2881. [CrossRef]
55. Park, J.S.; Kim, H.-S.; Hahn, H.T. Healing behavior of a matrix crack on a carbon fiber/mendomer composite. *Compos. Sci. Technol.* **2009**, *69*, 1082–1087. [CrossRef]
56. Murphy, E.B.; Bolanos, E.; Schaffner-Hamann, C.; Wudl, F.; Nutt, S.R.; Auad, M. Synthesis and Characterization of a Single-Component Thermally Remendable Polymer Network: Staudinger and Stille Revisited. *Macromolecules* **2008**, *41*, 5203–5209. [CrossRef]
57. Peterson, A.M.; Jensen, R.E.; Palmese, G.R. Reversibly Cross-Linked Polymer Gels as Healing Agents for Epoxy−Amine Thermosets. *ACS Appl. Mater. Interfaces* **2009**, *1*, 992–995. [CrossRef] [PubMed]
58. Chen, N.; Lee, Y.M. Anion exchange polyelectrolytes for membranes and ionomers. *Prog. Polym. Sci.* **2020**, *113*, 101345. [CrossRef]
59. Tanasi, P.; Santana, M.H.; Carretero-González, J.; Verdejo, R.; López-Manchado, M.A. Thermo-reversible crosslinked natural rubber: A Diels-Alder route for reuse and self-healing properties in elastomers. *Polymer* **2019**, *175*, 15–24. [CrossRef]
60. Eisenberg, A.; Rinaudo, M. Polyelectrolytes and ionomers. *Polym. Bull.* **1990**, *24*, 671. [CrossRef]
61. Cordier, P.; Tournilhac, F.; Soulié-Ziakovic, C.; Leibler, L. Self-healing and thermoreversible rubber from supramolecular assembly. *Nature* **2008**, *451*, 977–980. [CrossRef] [PubMed]
62. Montarnal, D.; Tournilhac, F.; Hidalgo, M.; Couturier, J.-L.; Leibler, L. Versatile One-Pot Synthesis of Supramolecular Plastics and Self-Healing Rubbers. *J. Am. Chem. Soc.* **2009**, *131*, 7966–7967. [CrossRef] [PubMed]
63. An, S.; Lee, M.W.; Yarin, A.L.; Yoon, S.S. A review on corrosion-protective extrinsic self-healing: Comparison of microcapsule-based systems and those based on core-shell vascular networks. *Chem. Eng. J.* **2018**, *344*, 206–220. [CrossRef]
64. Bakry, A.M.; Abbas, S.; Ali, B.; Majeed, H.; Abouelwafa, M.Y.; Mousa, A.; Liang, L. Microencapsulation of Oils: A Comprehensive Review of Benefits, Techniques, and Applications. *Compr. Rev. Food Sci. Food Saf.* **2015**, *15*, 143–182. [CrossRef]
65. Toohey, K.S.; Sottos, N.R.; Lewis, J.A.; Moore, J.; White, S. Self-healing materials with microvascular networks. *Nat. Mater.* **2007**, *6*, 581–585. [CrossRef] [PubMed]
66. Ullah, H.; Azizli, K.A.M.; Man, Z.B.; Ismail, M.B.C.; Khan, M.I. The Potential of Microencapsulated Self-healing Materials for Microcracks Recovery in Self-healing Composite Systems: A Review. *Polym. Rev.* **2016**, *56*, 429–485. [CrossRef]
67. Brown, E.N.; Sottos, N.R.; White, S.R. Fracture Testing of a Self-Healing Polymer Composite. *Exp. Mech.* **2002**, *42*, 372–379. [CrossRef]
68. Brown, E.; White, S.; Sottos, N. Retardation and repair of fatigue cracks in a microcapsule toughened epoxy composite—Part II: In situ self-healing. *Compos. Sci. Technol.* **2005**, *65*, 2474–2480. [CrossRef]
69. Keller, M.W.; White, S.R.; Sottos, N.R. A Self-Healing Poly(Dimethyl Siloxane) Elastomer. *Adv. Funct. Mater.* **2007**, *17*, 2399–2404. [CrossRef]
70. Kumar, A.; Stephenson, L.; Murray, J. Self-healing coatings for steel. *Prog. Org. Coat.* **2006**, *55*, 244–253. [CrossRef]
71. Caruso, M.M.; Delafuente, D.A.; Ho, V.; Sottos, N.R.; Moore, J.S.; White, S.R. Solvent-Promoted Self-Healing Epoxy Materials. *Macromolecules* **2007**, *40*, 8830–8832. [CrossRef]
72. Celestine, A.-D.N.; Sottos, N.R.; White, S.R. Autonomic healing of PMMA via microencapsulated solvent. *Polymer* **2015**, *69*, 241–248. [CrossRef]

73. White, S.R.; Moore, J.S.; Sottos, N.R.; Krull, B.P.; Cruz, W.A.S.; Gergely, R.C.R. Restoration of Large Damage Volumes in Polymers. *Science* **2014**, *344*, 620–623. [CrossRef]
74. Williams, G.; Trask, R.; Bond, I. A self-healing carbon fibre reinforced polymer for aerospace applications. *Compos. Part A Appl. Sci. Manuf.* **2007**, *38*, 1525–1532. [CrossRef]
75. Shields, Y.; De Belie, N.; Jefferson, A.; Van Tittelboom, K. A review of vascular networks for self-healing applications. *Smart Mater. Struct.* **2021**, *30*, 063001. [CrossRef]
76. Calderón-Villajos, R.; López, A.; Peponi, L.; Manzano-Santamaría, J.; Ureña, A. 3D-printed self-healing composite polymer reinforced with carbon nanotubes. *Mater. Lett.* **2019**, *249*, 91–94. [CrossRef]
77. Mondal, S.; Nguyen, T.P.; Pham, V.H.; Hoang, G.; Manivasagan, P.; Kim, M.H.; Nam, S.Y.; Oh, J. Hydroxyapatite nano bioceramics optimized 3D printed poly lactic acid scaffold for bone tissue engineering application. *Ceram. Int.* **2020**, *46*, 3443–3455. [CrossRef]
78. Caminero, M.Á.; Chacón, J.M.; García-Plaza, E.; Núñez, P.J.; Reverte, J.M.; Becar, J.P. Additive Manufacturing of PLA-Based Composites Using Fused Filament Fabrication: Effect of Graphene Nanoplatelet Reinforcement on Mechanical Properties, Dimensional Accuracy and Texture. *Polymers* **2019**, *11*, 799. [CrossRef] [PubMed]
79. Afif, A.; Rahman, S.M.; Azad, A.T.; Zaini, J.; Islam, A.; Azad, A. Advanced materials and technologies for hybrid supercapacitors for energy storage—A review. *J. Energy Storage* **2019**, *25*. [CrossRef]
80. Yu, K.; Xin, A.; Du, H.; Li, Y.; Wang, Q. Additive manufacturing of self-healing elastomers. *NPG Asia Mater.* **2019**, *11*, 7. [CrossRef]
81. Liu, S.; Li, L. Ultrastretchable and Self-Healing Double-Network Hydrogel for 3D Printing and Strain Sensor. *ACS Appl. Mater. Interfaces* **2017**, *9*, 26429–26437. [CrossRef] [PubMed]
82. Sanders, P.; Young, A.; Qin, Y.; Fancey, K.S.; Reithofer, M.R.; Guillet-Nicolas, R.; Kleitz, F.; Pamme, N.; Chin, J.M. Stereolithographic 3D printing of extrinsically self-healing composites. *Sci. Rep.* **2019**, *9*, 1–6. [CrossRef]
83. Postiglione, G.; Alberini, M.; Leigh, S.; Levi, M.; Turri, S. Effect of 3D-Printed Microvascular Network Design on the Self-Healing Behavior of Cross-Linked Polymers. *ACS Appl. Mater. Interfaces* **2017**, *9*, 14371–14378. [CrossRef]
84. Cheng, Y.; Chan, K.H.; Wang, X.-Q.; Ding, T.; Li, T.; Lu, X.; Ho, G.W. Direct-Ink-Write 3D Printing of Hydrogels into Biomimetic Soft Robots. *ACS Nano* **2019**, *13*, 13176–13184. [CrossRef] [PubMed]
85. Patel, D.; Sakhaei, A.H.; Layani, M.; Zhang, B.; Ge, Q.; Magdassi, S. Highly Stretchable and UV Curable Elastomers for Digital Light Processing Based 3D Printing. *Adv. Mater.* **2017**, *29*. [CrossRef] [PubMed]
86. Yap, H.K.; Ng, H.Y.; Yeow, C.-H. High-Force Soft Printable Pneumatics for Soft Robotic Applications. *Soft Robot.* **2016**, *3*, 144–158. [CrossRef]
87. Wang, Z.; Wang, Y.; Wang, Z.; He, Q.; Li, C.; Cai, S. 3D Printing of Electrically Responsive PVC Gel Actuators. *ACS Appl. Mater. Interfaces* **2021**, *13*, 24164–24172. [CrossRef] [PubMed]
88. Chortos, A.; Hajiesmaili, E.; Morales, J.; Clarke, D.R.; Lewis, J.A. 3D Printing of Interdigitated Dielectric Elastomer Actuators. *Adv. Funct. Mater.* **2019**, *30*. [CrossRef]
89. Lantean, S.; Barrera, G.; Pirri, C.F.; Tiberto, P.; Sangermano, M.; Roppolo, I.; Rizza, G. 3D Printing of Magnetoresponsive Polymeric Materials with Tunable Mechanical and Magnetic Properties by Digital Light Processing. *Adv. Mater. Technol.* **2019**, *4*. [CrossRef]
90. Yao, Y.; Yin, C.; Hong, S.; Chen, H.; Shi, Q.; Wang, J.; Lu, X.; Zhou, N. Lanthanide-Ion-Coordinated Supramolecular Hydrogel Inks for 3D Printed Full-Color Luminescence and Opacity-Tuning Soft Actuators. *Chem. Mater.* **2020**, *32*, 8868–8876. [CrossRef]
91. Cho, K.; Kang, D.; Lee, H.; Koh, W.-G. Multi-stimuli responsive and reversible soft actuator engineered by layered fibrous matrix and hydrogel micropatterns. *Chem. Eng. J.* **2021**, *427*, 130879. [CrossRef]
92. Kokkinis, D.; Schaffner, M.; Studart, A.R. Multimaterial magnetically assisted 3D printing of composite materials. *Nat. Commun.* **2015**, *6*, 8643. [CrossRef] [PubMed]
93. Odent, J.; Vanderstappen, S.; Toncheva, A.; Pichon, E.; Wallin, T.J.; Wang, K.; Shepherd, R.F.; Dubois, P.; Raquez, J.-M. Hierarchical chemomechanical encoding of multi-responsive hydrogel actuators via 3D printing. *J. Mater. Chem. A* **2019**, *7*, 15395–15403. [CrossRef]
94. Zhou, F.; Zhang, M.; Cao, X.; Zhang, Z.; Chen, X.; Xiao, Y.; Liang, Y.; Wong, T.-W.; Li, T.; Xu, Z. Fabrication and modeling of dielectric elastomer soft actuator with 3D printed thermoplastic frame. *Sens. Actuators A Phys.* **2019**, *292*, 112–120. [CrossRef]
95. Wang, Z.; Gao, W.; Zhang, Q.; Zheng, K.; Xu, J.; Xu, W.; Shang, E.; Jiang, J.; Zhang, J.; Liu, Y. 3D-Printed Graphene/Polydimethylsiloxane Composites for Stretchable and Strain-Insensitive Temperature Sensors. *ACS Appl. Mater. Interfaces* **2018**, *11*, 1344–1352. [CrossRef] [PubMed]
96. Kalsoom, U.; Waheed, S.; Paull, B. Fabrication of Humidity Sensor Using 3D Printable Polymer Composite Containing Boron-Doped Diamonds and LiCl. *ACS Appl. Mater. Interfaces* **2020**, *12*, 4962–4969. [CrossRef] [PubMed]
97. Mu, Q.; Wang, L.; Dunn, C.K.; Kuang, X.; Duan, F.; Zhang, Z.; Qi, H.J.; Wang, T. Digital light processing 3D printing of conductive complex structures Digital light processing 3D printing of conductive complex structures. *Addit. Manuf.* **2017**, *18*, 74–83. [CrossRef]
98. Shen, K.; Ding, J.; Yang, S. 3D Printing Quasi-Solid-State Asymmetric Micro-Supercapacitors with Ultrahigh Areal Energy Density. *Adv. Energy Mater.* **2018**, *8*. [CrossRef]
99. Park, S.H.; Kaur, M.; Yun, D.; Kim, W.S. Hierarchically Designed Electron Paths in 3D Printed Energy Storage Devices. *Langmuir* **2018**, *34*, 10897–10904. [CrossRef] [PubMed]
100. McOwen, D.W.; Xu, S.; Gong, Y.; Wen, Y.; Godbey, G.L.; Gritton, J.; Hamann, T.R.; Dai, J.; Hitz, G.T.; Hu, L.; et al. 3D-Printing Electrolytes for Solid-State Batteries. *Adv. Mater.* **2018**, *30*, e1707132. [CrossRef] [PubMed]

101. He, Y.; Chen, S.; Nie, L.; Sun, Z.; Wu, X.; Liu, W. Stereolithography Three-Dimensional Printing Solid Polymer Electrolytes for All-Solid-State Lithium Metal Batteries. *Nano Lett.* **2020**, *20*, 7136–7143. [CrossRef] [PubMed]
102. Ayan, B.; Heo, D.N.; Zhang, Z.; Dey, M.; Povilianskas, A.; Drapaca, C.; Ozbolat, I.T. Aspiration-assisted bioprinting for precise positioning of biologics. *Sci. Adv.* **2020**, *6*, eaaw5111. [CrossRef]
103. Katzschmann, R.K.; Marchese, A.D.; Rus, D. Hydraulic Autonomous Soft Robotic Fish for 3D Swimming. *Exp. Robot.* **2015**, 405–420. [CrossRef]
104. Zhu, M.; Do, T.N.; Hawkes, E.; Visell, Y. Fluidic Fabric Muscle Sheets for Wearable and Soft Robotics. *Soft Robot.* **2020**, *7*, 179–197. [CrossRef]
105. MacCurdy, R.; Katzschmann, R.; Kim, Y.; Rus, D. Printable hydraulics: A method for fabricating robots by 3D co-printing solids and liquids. In Proceedings of the 2016 IEEE International Conference on Robotics and Automation (ICRA), Stockholm, Sweden, 16–21 May 2016; pp. 3878–3885.
106. Zatopa, A.; Walker, S.; Menguc, Y. Fully Soft 3D-Printed Electroactive Fluidic Valve for Soft Hydraulic Robots. *Soft Robot.* **2018**, *5*, 258–271. [CrossRef] [PubMed]
107. O'Neill, M.R.; Acome, E.; Bakarich, S.; Mitchell, S.K.; Timko, J.; Keplinger, C.; Shepherd, R.F. Rapid 3D Printing of Electrohydraulic (HASEL) Tentacle Actuators. *Adv. Funct. Mater.* **2020**, *30*, 2005244. [CrossRef]
108. Lee, C.; Kim, M.; Kim, Y.J.; Hong, N.; Ryu, S.; Kim, H.J.; Kim, S. Soft robot review. *Int. J. Control. Autom. Syst.* **2017**, *15*, 3–15. [CrossRef]
109. Peele, B.N.; Wallin, T.J.; Zhao, H.; Shepherd, R. 3D printing antagonistic systems of artificial muscle using projection stereolithography. *Bioinspiration Biomimetics* **2015**, *10*, 055003. [CrossRef] [PubMed]
110. Keong, B.A.W.; Hua, R.Y.C. A Novel Fold-Based Design Approach toward Printable Soft Robotics Using Flexible 3D Printing Materials. *Adv. Mater. Technol.* **2017**, *3*. [CrossRef]
111. Zhang, Y.; Ng, C.J.; Chen, Z.; Zhang, W.; Panjwani, S.; Kowsari, K.; Yang, H.Y.; Ge, Q. Miniature Pneumatic Actuators for Soft Robots by High-Resolution Multimaterial 3D Printing. *Adv. Mater. Technol.* **2019**, *4*, 1900427. [CrossRef]
112. Zhang, Y.; Zhang, N.; Hingorani, H.; Ding, N.; Wang, D.; Yuan, C.; Zhang, B.; Gu, G.; Ge, Q. Fast-Response, Stiffness-Tunable Soft Actuator by Hybrid Multimaterial 3D Printing. *Adv. Funct. Mater.* **2019**, *29*. [CrossRef]
113. Thrasher, C.J.; Schwartz, J.J.; Boydston, A.J. Modular Elastomer Photoresins for Digital Light Processing Additive Manufacturing. *ACS Appl. Mater. Interfaces* **2017**, *9*, 39708–39716. [CrossRef]
114. Ge, Q.; Chen, Z.; Cheng, J.; Zhang, B.; Zhang, Y.-F.; Li, H.; He, X.; Yuan, C.; Liu, J.; Magdassi, S.; et al. 3D printing of highly stretchable hydrogel with diverse UV curable polymers. *Sci. Adv.* **2021**, *7*, eaba4261. [CrossRef]
115. Sellinger, A.T.; Wang, D.H.; Tan, L.-S.; Vaia, R.A. Electrothermal Polymer Nanocomposite Actuators. *Adv. Mater.* **2010**, *22*, 3430–3435. [CrossRef]
116. Zhang, T.-Y.; Wang, Q.; Deng, N.-Q.; Zhao, H.-M.; Wang, D.-Y.; Yang, Z.; Liu, Y.; Yang, Y.; Ren, T.-L. A large-strain, fast-response, and easy-to-manufacture electrothermal actuator based on laser-reduced graphene oxide. *Appl. Phys. Lett.* **2017**, *111*, 121901. [CrossRef]
117. Sachyani Keneth, E.; Scalet, G.; Layani, M.; Tibi, G.; Degani, A.; Auricchio, F.; Magdassi, S. Pre-Programmed Tri-Layer Electro-Thermal Actuators Composed of Shape Memory Polymer and Carbon Nanotubes. *Soft Robot.* **2020**, *7*, 123–129. [CrossRef] [PubMed]
118. Chen, Y.; Agostini, L.; Moretti, G.; Fontana, M.; Vertechy, R. Dielectric elastomer materials for large-strain actuation and energy harvesting: A comparison between styrenic rubber, natural rubber and acrylic elastomer. *Smart Mater. Struct.* **2019**, *28*, 114001. [CrossRef]
119. Chiba, S. Dielectric elastomers. In *Soft Actuators: Materials, Modeling, Applications, and Future Perspectives*; Springer: Tokyo, Japan, 2014; Volume 9784431547, pp. 183–195.
120. Suo, Z. Theory of dielectric elastomers. *Acta Mech. Solida Sin.* **2010**, *23*, 549–578. [CrossRef]
121. Wang, T.; Farajollahi, M.; Choi, Y.S.; Lin, I.-T.; Marshall, J.E.; Thompson, N.M.; Kar-Narayan, S.; Madden, J.D.W.; Smoukov, S.K. Electroactive polymers for sensing. *Interface Focus* **2016**, *6*, 20160026. [CrossRef] [PubMed]
122. Shang, Y.; Wang, J.; Ikeda, T.; Jiang, L. Bio-inspired liquid crystal actuator materials. *J. Mater. Chem. C* **2019**, *7*, 3413–3428. [CrossRef]
123. Hines, L.; Petersen, K.H.; Lum, G.Z.; Sitti, M. Soft Actuators for Small-Scale Robotics. *Adv. Mater.* **2017**, *29*, 1603483. [CrossRef] [PubMed]
124. Terasawa, N.; Ono, N.; Mukai, K.; Koga, T.; Higashi, N.; Asaka, K. A multi-walled carbon nanotube/polymer actuator that surpasses the performance of a single-walled carbon nanotube/polymer actuator. *Carbon* **2012**, *50*, 311–320. [CrossRef]
125. Wang, B.; Hong, L.; Li, Y.; Zhao, L.; Zhao, C.; Na, H. Property Enhancement Effects of Side-Chain-Type Naphthalene-Based Sulfonated Poly(arylene ether ketone) on Nafion Composite Membranes for Direct Methanol Fuel Cells. *ACS Appl. Mater. Interfaces* **2017**, *9*, 32227–32236. [CrossRef] [PubMed]
126. Keneth, E.S.; Kamyshny, A.; Totaro, M.; Beccai, L.; Magdassi, S. 3D Printing Materials for Soft Robotics. *Adv. Mater.* **2020**, *33*, e2003387. [CrossRef]
127. Han, D.; Farino, C.; Yang, C.; Scott, T.; Browe, D.; Choi, W.; Freeman, J.W.; Lee, H. Soft Robotic Manipulation and Locomotion with a 3D Printed Electroactive Hydrogel. *ACS Appl. Mater. Interfaces* **2018**, *10*, 17512–17518. [CrossRef] [PubMed]

128. Shin, Y.; Choi, M.-Y.; Choi, J.; Na, J.-H.; Kim, S.Y. Design of an Electro-Stimulated Hydrogel Actuator System with Fast Flexible Folding Deformation under a Low Electric Field. *ACS Appl. Mater. Interfaces* **2021**, *13*, 15633–15646. [CrossRef] [PubMed]
129. Sommer-Larsen, P.; Kofod, G.; Shridhar, M.H.; Benslimane, M.; Gravesen, P. Performance of dielectric elastomer actuators and materials. *SPIE Proc.* **2002**, *4695*, 158–166. [CrossRef]
130. Gupta, U.; Qin, L.; Wang, Y.; Godaba, H.; Zhu, J. Soft robots based on dielectric elastomer actuators: A review. *Smart Mater. Struct.* **2019**, *28*, 103002. [CrossRef]
131. Zhang, J.; Sheng, J.; O'Neill, C.T.; Walsh, C.J.; Wood, R.J.; Ryu, J.-H.; Desai, J.P.; Yip, M.C. Robotic Artificial Muscles: Current Progress and Future Perspectives. *IEEE Trans. Robot.* **2019**, *35*, 761–781. [CrossRef]
132. Correia, D.; Fernandes, L.; Pereira, N.; Barbosa, J.; Serra, J.; Pinto, R.; Costa, C.; Lanceros-Méndez, S. All printed soft actuators based on ionic liquid/polymer hybrid materials. *Appl. Mater. Today* **2021**, *22*, 100928. [CrossRef]
133. Correia, D.M.; Barbosa, J.C.; Serra, J.P.; Pinto, R.S.; Fernandes, L.C.; Tubio, C.R.; Lanceros-Mendez, S.; Costa, C.M. Comparative Assessment of Ionic Liquid-Based Soft Actuators Prepared by Film Casting Versus Direct Ink Writing. *Adv. Eng. Mater.* **2021**, *23*, 2100411. [CrossRef]
134. Maas, J.; Tepel, D.; Hoffstadt, T. Actuator design and automated manufacturing process for DEAP-based multilayer stack-actuators. *Meccanica* **2015**, *50*, 2839–2854. [CrossRef]
135. Ralchev, M.; Mateev, V.; Marinova, I. Magnetic Properties of FFF/FDM 3D Printed Magnetic Material. In Proceedings of the Conference on Electrical Machines, Drives and Power Systems (ELMA), Sofia, Bulgaria, 1–4 July 2021; pp. 1–5. [CrossRef]
136. Ji, Z.; Yan, C.; Yu, B.; Wang, X.; Zhou, F. Multimaterials 3D Printing for Free Assembly Manufacturing of Magnetic Driving Soft Actuator. *Adv. Mater. Interfaces* **2017**, *4*. [CrossRef]
137. Richbourg, N.R.; Peppas, N.A. The swollen polymer network hypothesis: Quantitative models of hydrogel swelling, stiffness, and solute transport. *Prog. Polym. Sci.* **2020**, *105*, 101243. [CrossRef]
138. Lopez, C.G.; Lohmeier, T.; Wong, J.E.; Richtering, W. Electrostatic expansion of polyelectrolyte microgels: Effect of solvent quality and added salt. *J. Colloid Interface Sci.* **2019**, *558*, 200–210. [CrossRef] [PubMed]
139. Peppas, N.A.; Reinhart, C.T. Solute diffusion in swollen membranes. Part I. A new theory. *J. Membr. Sci.* **1983**, *15*, 275–287. [CrossRef]
140. Dutta, S.; Cohn, D. Temperature and pH responsive 3D printed scaffolds. *J. Mater. Chem. B* **2017**, *5*, 9514–9521. [CrossRef] [PubMed]
141. Chang, Q.; Darabi, M.A.; Liu, Y.; He, Y.; Zhong, W.; Mequanin, K.; Li, B.; Lu, F.; Xing, M.M.Q. Hydrogels from natural egg white with extraordinary stretchability, direct-writing 3D printability and self-healing for fabrication of electronic sensors and actuators. *J. Mater. Chem. A* **2019**, *7*, 24626–24640. [CrossRef]
142. Bakarich, S.E.; Gorkin, R.; Panhuis, M.I.H.; Spinks, G.M. 4D Printing with Mechanically Robust, Thermally Actuating Hydrogels. *Macromol. Rapid Commun.* **2015**, *36*, 1211–1217. [CrossRef] [PubMed]
143. DI Noto, V.; Lavina, S.; Giffin, G.; Negro, E.; Scrosati, B. Polymer electrolytes: Present, past and future. *Electrochim. Acta* **2011**, *57*, 4–13. [CrossRef]
144. Su, M.; Song, Y. Printable Smart Materials and Devices: Strategies and Applications. *Chem. Rev.* **2022**, *122*, 5144–5164. [CrossRef] [PubMed]
145. Muth, J.T.; Vogt, D.M.; Truby, R.L.; Mengüç, Y.; Kolesky, D.B.; Wood, R.J.; Lewis, J.A. Embedded 3D Printing of Strain Sensors within Highly Stretchable Elastomers. *Adv. Mater.* **2014**, *26*, 6307–6312. [CrossRef] [PubMed]
146. Jiang, Y.; Ma, J.; Lv, J.; Ma, H.; Xia, H.; Wang, J.; Yang, C.; Xue, M.; Li, G.; Zhu, N. Facile Wearable Vapor/Liquid Amphibious Methanol Sensor. *ACS Sens.* **2018**, *4*, 152–160. [CrossRef]
147. Plevniak, K.; Campbell, M.; Myers, T.; Hodges, A.; He, M. 3D printed auto-mixing chip enables rapid smartphone diagnosis of anemia. *Biomicrofluidics* **2016**, *10*, 054113. [CrossRef]
148. Yang, W.; Yang, J.; Byun, J.J.; Moissinac, F.P.; Xu, J.; Haigh, S.J.; Domingos, M.; Bissett, M.A.; Dryfe, R.A.W.; Barg, S. 3D Printing of Freestanding MXene Architectures for Current-Collector-Free Supercapacitors. *Adv. Mater.* **2019**, *31*, 1902725. [CrossRef] [PubMed]
149. Mai, H.N.; Lee, K.-B.; Lee, D.-H. Fit of interim crowns fabricated using photopolymer-jetting 3D printing. *J. Prosthet. Dent.* **2017**, *118*, 208–215. [CrossRef]
150. Moncal, K.K.; Gudapati, H.; Godzik, K.P.; Heo, D.N.; Kang, Y.; Rizk, E.; Ravnic, D.J.; Wee, H.; Pepley, D.F.; Ozbolat, V.; et al. Intra-Operative Bioprinting of Hard, Soft, and Hard/Soft Composite Tissues for Craniomaxillofacial Reconstruction. *Adv. Funct. Mater.* **2021**, *31*, 2010858. [CrossRef] [PubMed]
151. Chen, W.; Yan, X. Progress in achieving high-performance piezoresistive and capacitive flexible pressure sensors: A review. *J. Mater. Sci. Technol.* **2020**, *43*, 175–188. [CrossRef]
152. Zhou, N.; Liu, T.; Wen, B.; Gong, C.; Wei, G.; Su, Z. Recent Advances in the Construction of Flexible Sensors for Biomedical Applications. *Biotechnol. J.* **2020**, *15*. [CrossRef] [PubMed]
153. Trung, T.Q.; Ramasundaram, S.; Hwang, B.-U.; Lee, N.-E. An All-Elastomeric Transparent and Stretchable Temperature Sensor for Body-Attachable Wearable Electronics. *Adv. Mater.* **2015**, *28*, 502–509. [CrossRef]
154. Di, J.; Zhang, X.; Yong, Z.; Zhang, Y.; Li, D.; Li, R.; Li, Q. Carbon-Nanotube Fibers for Wearable Devices and Smart Textiles. *Adv. Mater.* **2016**, *28*, 10529–10538. [CrossRef] [PubMed]

155. Wang, Z.; Liu, X.; Shen, X.; Han, N.M.; Wu, Y.; Zheng, Q.; Jia, J.; Wang, N.; Kim, J. An Ultralight Graphene Honeycomb Sandwich for Stretchable Light-Emitting Displays. *Adv. Funct. Mater.* **2018**, *28*. [CrossRef]
156. Xiao, T.; Qian, C.; Yin, R.; Wang, K.; Gao, Y.; Xuan, F. 3D Printing of Flexible Strain Sensor Array Based on UV-Curable Multiwalled Carbon Nanotube/Elastomer Composite. *Adv. Mater. Technol.* **2020**, *6*. [CrossRef]
157. Wu, T.; Gray, E.; Chen, B. A self-healing, adaptive and conductive polymer composite ink for 3D printing of gas sensors. *J. Mater. Chem. C* **2018**, *6*, 6200–6207. [CrossRef]
158. Han, T.; Kundu, S.; Nag, A.; Xu, Y. 3D Printed Sensors for Biomedical Applications: A Review. *Sensors* **2019**, *19*, 1706. [CrossRef] [PubMed]
159. Wang, Z.; Liu, J.; Wang, M.; Shen, X.; Qian, T.; Yan, C. Toward safer solid-state lithium metal batteries: A review. *Nanoscale Adv.* **2020**, *2*, 1828–1836. [CrossRef]
160. Li, S.; Zhang, S.; Shen, L.; Liu, Q.; Ma, J.; Lv, W.; He, Y.; Yang, Q. Progress and Perspective of Ceramic/Polymer Composite Solid Electrolytes for Lithium Batteries. *Adv. Sci.* **2020**, *7*, 1903088. [CrossRef] [PubMed]
161. Li, Y.; Li, Q.; Tan, Z. A review of electrospun nanofiber-based separators for rechargeable lithium-ion batteries. *J. Power Sources* **2019**, *443*, 227262. [CrossRef]
162. Wei, T.; Ahn, B.Y.; Grotto, J.; Lewis, J.A. 3D Printing of Customized Li-Ion Batteries with Thick Electrodes. *Adv. Mater.* **2018**, *30*, e1703027. [CrossRef] [PubMed]
163. Shen, W.; Li, K.; Lv, Y.; Xu, T.; Wei, D.; Liu, Z. Highly-Safe and Ultra-Stable All-Flexible Gel Polymer Lithium Ion Batteries Aiming for Scalable Applications. *Adv. Energy Mater.* **2020**, *10*. [CrossRef]
164. Deiner, L.J.; Bezerra, C.A.G.; Howell, T.G.; Powell, A.S. Digital Printing of Solid-State Lithium-Ion Batteries. *Adv. Eng. Mater.* **2019**, *21*, 1900737. [CrossRef]
165. Poly(Ethylene Oxide)−LiTFSI Solid Polymer Electrolyte Filaments. *J. Electrochem. Soc.* **2020**, *167*, 7.
166. Zhang, Y.; Ji, T.; Hou, S.; Zhang, L.; Shi, Y.; Zhao, J.; Xu, X. All-printed solid-state substrate-versatile and high-performance micro-supercapacitors for in situ fabricated transferable and wearable energy storage via multi-material 3D printing. *J. Power Sources* **2018**, *403*, 109–117. [CrossRef]
167. Areir, M.; Xu, Y.; Harrison, D.; Fyson, J. 3D printing of highly flexible supercapacitor designed for wearable energy storage. *Mater. Sci. Eng. B* **2017**, *226*, 29–38. [CrossRef]
168. Khorsandi, D.; Fahimipour, A.; Abasian, P.; Saber, S.S.; Seyedi, M.; Ghanavati, S.; Ahmad, A.; De Stephanis, A.A.; Taghavinezhaddilami, F.; Leonova, A.; et al. 3D and 4D printing in dentistry and maxillofacial surgery: Printing techniques, materials, and applications. *Acta Biomater.* **2020**, *122*, 26–49. [CrossRef] [PubMed]
169. Xu, X.; Awad, A.; Robles-Martinez, P.; Gaisford, S.; Goyanes, A.; Basit, A.W. Vat photopolymerization 3D printing for advanced drug delivery and medical device applications. *J. Control. Release* **2020**, *329*, 743–757. [CrossRef] [PubMed]
170. Werz, S.M.; Zeichner, S.J.; Berg, B.-I.; Zeilhofer, H.-F.; Thieringer, F. 3D Printed Surgical Simulation Models as educational tool by maxillofacial surgeons. *Eur. J. Dent. Educ.* **2018**, *22*, e500–e505. [CrossRef]
171. Shon, H.C.; Bang, J.-Y.; Lee, Y.; Koh, K.H.; Kim, J.W. Optimal plate position in minimally invasive plate osteosynthesis for mid-shaft clavicle fractures: Simulation using 3D-printed models of actual clinical cases. *Eur. J. Trauma Emerg. Surg.* **2020**, *47*, 1411–1416. [CrossRef] [PubMed]
172. Zhou, H.; Tawk, C.; Alici, G. A 3D Printed Soft Prosthetic Hand with Embedded Actuation and Soft Sensing Capabilities for Directly and Seamlessly Switching Between Various Hand Gestures. In Proceedings of the IEEE/ASME International Conference on Advanced Intelligent Mechatronics (AIM), Delft, The Netherlands, 12–16 July 2021; pp. 75–80. [CrossRef]
173. Beheshtizadeh, N.; Lotfibakhshaiesh, N.; Pazhouhnia, Z.; Hoseinpour, M.; Nafari, M. A review of 3D bio-printing for bone and skin tissue engineering: A commercial approach. *J. Mater. Sci.* **2019**, *55*, 3729–3749. [CrossRef]
174. Ning, L.; Chen, X.; Ning, L. A brief review of extrusion-based tissue scaffold bio-printing. *Biotechnol. J.* **2017**, *12*. [CrossRef]
175. Mercado-Pagán, E.; Stahl, A.M.; Shanjani, Y.; Yang, Y. Vascularization in Bone Tissue Engineering Constructs. *Ann. Biomed. Eng.* **2015**, *43*, 718–729. [CrossRef] [PubMed]
176. Guddati, S.; Kiran, A.S.K.; Leavy, M.; Ramakrishna, S. Recent advancements in additive manufacturing technologies for porous material applications. *Int. J. Adv. Manuf. Technol.* **2019**, *105*, 193–215. [CrossRef]
177. Almetwally, A.G.; Jabbari, H. 3D-Printing Replication of Porous Media for Lab-Scale Characterization Research. *ACS Omega* **2021**, *6*, 2655–2664. [CrossRef]
178. Ozelim, L.C.D.S.M.; Cavalcante, A.L.B. Combining Microtomography, 3D Printing, and Numerical Simulations to Study Scale Effects on the Permeability of Porous Media. *Int. J. Géoméch.* **2019**, *19*, 04018194. [CrossRef]
179. Suzuki, A.; Watanabe, N.; Li, K.; Horne, R.N. Fracture network created by 3-D printer and its validation using CT images. *Water Resour. Res.* **2017**, *53*, 6330–6339. [CrossRef]
180. Bacher, M.; Schwen, A.; Koestel, J. Three-Dimensional Printing of Macropore Networks of an Undisturbed Soil Sample. *Vadose Zone J.* **2015**, *14*. [CrossRef]
181. Ferro, N.D.; Morari, F. From Real Soils to 3D-Printed Soils: Reproduction of Complex Pore Network at the Real Size in a Silty-Loam Soil. *Soil Sci. Soc. Am. J.* **2015**, *79*, 1008–1017. [CrossRef]
182. Anjikar, I.S.; Wales, S.; Beckingham, L.E. Fused Filament Fabrication 3-D Printing of Reactive Porous Media. *Geophys. Res. Lett.* **2020**, *47*. [CrossRef]
183. Ishutov, S.; Hasiuk, F.; Harding, C.; Gray, J.N. 3D printing sandstone porosity models. *Interpretation* **2015**, *3*, SX49–SX61. [CrossRef]

184. Goral, J.; Deo, M. Nanofabrication of synthetic nanoporous geomaterials: From nanoscale-resolution 3D imaging to nano-3D-printed digital (shale) rock. *Sci. Rep.* **2020**, *10*, 1–12. [CrossRef]
185. Garum, M.; Glover, P.W.J.; Lorinczi, P.; Scott, G.; Hassanpour, A. Ultrahigh-Resolution 3D Imaging for Quantifying the Pore Nanostructure of Shale and Predicting Gas Transport. *Energy Fuels* **2020**, *35*, 702–717. [CrossRef]
186. Almetwally, A.; Jabbari, H. Experimental investigation of 3D printed rock samples replicas. *J. Nat. Gas Sci. Eng.* **2020**, *76*, 103192. [CrossRef]
187. Ishutov, S.; Hasiuk, F.J.; Jobe, D.; Agar, S. Using Resin-Based 3D Printing to Build Geometrically Accurate Proxies of Porous Sedimentary Rocks. *Groundwater* **2017**, *56*, 482–490. [CrossRef]
188. Song, R.; Wang, Y.; Sun, S.; Liu, J. Characterization and microfabrication of natural porous rocks: From micro-CT imaging and digital rock modelling to micro-3D-printed rock analogs. *J. Pet. Sci. Eng.* **2021**, *205*, 108827. [CrossRef]
189. Kong, L.; Ostadhassan, M.; Hou, X.; Mann, M.; Li, C. Microstructure characteristics and fractal analysis of 3D-printed sandstone using micro-CT and SEM-EDS. *J. Pet. Sci. Eng.* **2019**, *175*, 1039–1048. [CrossRef]
190. Head, D.; Vanorio, T. Effects of changes in rock microstructures on permeability: 3-D printing investigation. *Geophys. Res. Lett.* **2016**, *43*, 7494–7502. [CrossRef]
191. Jiang, C.; Zhao, G.-F. A Preliminary Study of 3D Printing on Rock Mechanics. *Rock Mech. Rock Eng.* **2014**, *48*, 1041–1050. [CrossRef]
192. Jiang, Q.; Feng, X.; Song, L.; Gong, Y.; Zheng, H.; Cui, J. Modeling rock specimens through 3D printing: Tentative experiments and prospects. *Acta Mech. Sin.* **2015**, *32*, 101–111. [CrossRef]
193. Hodder, K.J.; Nychka, J.A.; Chalaturnyk, R.J. Process limitations of 3D printing model rock. *Prog. Addit. Manuf.* **2018**, *3*, 173–182. [CrossRef]